TAMPEREEN TEKNILLINEN YLIOPISTO

TUUVA KASTINEN

DOUBLE MELTING BEHAVIOUR AND PLASTICIZATION OF POLYLACTIC ACID - A TOPEM AND FTIR STUDY

Master of Science Thesis

Examiners:
Adj. Prof. Terttu Hukka
Professor Helge Lemmetyinen
Examiners and topic approved in
the Faculty Council meeting of the
Faculty of Science and Environmental
Engineering on February 8th 2012

ABSTRACT

TAMPERE UNIVERSITY OF TECHNOLOGY
Master's Degree Programme in Science and Engineering
KASTINEN, TUUVA: **Double Melting Behavior and Plasticization of Polylactic acid – a TOPEM and FTIR Study**
Master of Science Thesis, 73 pages
June 2012
Major: Chemistry
Examiners: Adj. Prof. Terttu Hukka, Professor Helge Lemmetyinen
Keywords: double melting behavior, polylactic acid, TOPEM, plasticization

The multiple melting behavior is a common phenomenon observed by differential scanning calorimetry (DSC) for polymorphic polymers. In the case of poly(lactic acid) (PLA) this is detected as double melting peaks, which have been proposed to arise from α- and α'- crystalline forms of the polymer. Various explanations have been presented for the mechanism behind this behavior, namely melt-recrystallization, multiple lamellae population and multiple crystal structure, but so far none of them has been fully confirmed.

Determination of the thermal properties of PLA is crucial, because the polymer is used as a material for medical applications alongside food packaging. PLA is known to degrade via hydrolysis under certain thermal and humidity conditions, for which reason the degradation time and rate should be taken into account. At body temperature the plasticizing effect of water can be utilized in the activation of the shape-memory of amorphous poly(D,L-lactic acid) (PDLLA).

In this thesis, an investigation of the double melting behavior of the poly(L,D-lactic acid) (P(L/D)LA) samples with two different D-contents by a new temperature-modulated differential scanning calorimetry (TMDSC) method, TOPEM is presented. The aim of the study is to determine the suitable parameters for TOPEM studies in the melting region and establish, whether this method is convenient to measure the phenomenon in question. The other part of the study concentrates on the examination of the plasticizing effect of water by Fourier transform infrared (FTIR) spectroscopy. In addition, the effect of gamma sterilization on the dry and wet samples is investigated.

The results obtained by TOPEM correlate well with the ones attained by the conventional DSC method. The required crystallization temperature and time for the appearance of double melting peaks in the DSC curves are different for the samples with different D-contents. In both cases, the major part of melting is observed to be non-reversing. This is explained by superheating of the samples, which is assumed to be due to the slow melting kinetics during TOPEM measurements. Reversible melting in turn occurs simultaneously with the crystallization process, which is detected in the non-reversing heat flow curve. This supports the melting-recrystallization model suggested in previous studies.

The plasticizing effect of water is observed clearly in certain IR-absorption bands in the region of 3800–3400 cm^{-1}. A new band appearing in the region of 1700–1500 cm^{-1} is assigned to the bending mode of free water present in the samples. The changes in the spectra indicate that PLA degrades because of water treatment. Gamma sterilization, in turn, is not observed to have significant effect on the bands. Further investigation would be required to determine, whether this is due to alternating quality and thickness of the samples.

TIIVISTELMÄ

TAMPEREEN TEKNILLINEN YLIOPISTO
Teknis-luonnontieteellinen koulutusohjelma
KASTINEN, TUUVA: **Polylaktidin kaksoissulamiskäyttäytyminen ja veden plastisoiva vaikutus - TOPEM ja FTIR tutkimus**
Diplomityö, 73 sivua
Kesäkuu 2012
Pääaine: Kemia
Tarkastajat: dosentti Terttu Hukka, professori Helge Lemmetyinen
Avainsanat: kaksoissulaminen, polylaktidi, DSC, TOPEM, plastisointi, FTIR

Moninkertainen sulamiskäyttäytyminen on polymorfisilla polymeereillä yleisesti havaittava ilmiö. Polylaktidin (PLA) tapauksessa tämä nähdään kahtena sulamispiikkinä, joiden on esitetty olevan lähtöisin polymeerin α- ja α'-kidemuodoista. Kyseiselle mekanismille on esitetty useampia selityksiä, kuten sulamis-uudelleenkiteytyminen, moninkertainen lamellipopulaatio ja moninkertainen kiderakenne, mutta yhtäkään niistä ei ole tähän mennessä vielä täysin vahvistettu.

Koska PLA:ta käytetään materiaalina ruokapakkauksissa ja lääketieteellisissä sovelluksissa, on tärkeää ymmärtää sen termiset ominaisuudet. PLA:n tiedetään hajoavan hydrolyyttisesti sopivissa lämpötila- ja kosteusolosuhteissa, minkä takia hajoamiseen vaadittava aika ja nopeus tulisi ottaa huomioon. Kehon lämpötilassa veden plastisoivaa vaikutusta voidaan hyödyntää amorfisen poly(D,L-laktidin) (PDLLA) muotomuistin aktivoinnissa.

Tässä diplomityössä on tutkittu kahden stereokemialliselta koostumukseltaan erilaisen poly(L,D-laktidi) (P(L/D)LA)-näytteen kaksoissulamiskäyttäytymistä uudella lämpötilamoduloidulla pyyhkäisykalorimetrialla (TMDSC), TOPEM:illa. Tavoitteena on ollut määrittää sopivat parametrit TOPEM-mittauksia varten sulamisalueelle ja selvittää, onko kyseinen menetelmä sopiva kaksoissulamiskäyttäytymisen tutkimiseen. Työn toinen osio keskittyy veden plastisoivan vaikutuksen selvittämiseen Fourier-muunnos infrapuna (FTIR) spektrometrilla. Lisäksi tarkastellaan gammasteriloinnin vaikutusta kuiviin ja kosteisiin näytteisiin.

TOPEM:illa saadut tulokset vastaavat hyvin perinteisellä DSC-menetelmällä saatuja tuloksia. Kaksoissulamispiikkien esiintymiseen vaadittava kiteytymislämpötila ja -aika vaihtelevat näytteen sisältämän D-enantiomeerin mukaan. Molemmissa tapauksissa suurimman osan sulamisesta havaitaan olevan palautumatonta. Tämän selittää näytteiden ylikuumeneminen, jonka voidaan olettaa johtuvan hitaasta sulamiskinetiikasta TOPEM-mittausten aikana. Palautuva sulaminen puolestaan tapahtuu samanaikaisesti irreversiibelillä DSC-käyrällä havaittavan kiteytymisen kanssa. Tämä tukee aiemmissa tutkimuksissa esitettyä sulamis-uudelleenkiteytymismallia.

Veden plastisoiva vaikutus havaitaan selkeästi tietyissä IR-absorptiovöissä alueella 3700–3500 cm^{-1}. Alueelle 1636–1625 cm^{-1} ilmestyvä uusi absorptiovyö voidaan yhdistää näytteessä olevan vapaan veden taivutusvärähdyksiin. Muutokset spektreissä viittaavat siihen, että PLA hajoaa vesikäsittelyn vaikutuksesta. Gammasterilisoinnilla ei puolestaan havaita olevan huomattavaa vaikutusta piikkeihin. Jatkotutkimuksia tarvittaisiin selvittämään, johtuuko tämä näytteiden vaihtelevasta laadusta ja paksuudesta.

PREFACE

This Master of Science Thesis was done at the Department of Chemistry and Bioengineering at Tampere University of Technology. The studies for the thesis were performed at the Chemistry laboratory between September 2011 and February 2012. The Chemistry laboratory is gratefully acknowledged for funding this work.

First, I would like to thank my supervisor Adj. Prof., Dr. Terttu Hukka for the opportunity to perform this thesis and all the invaluable guidance and support I received throughout this work. I appreciate the time and patience she always had for all my questions. I am grateful to the examiner of my M.Sc. thesis, Head of the Laboratory, Prof. Helge Lemmetyinen, for all the advice provided. M.Sc. Sanna-Maarit Auvinen and Lic. Phil. Sami Kotkamo are acknowledged for providing the PLA samples. I thank also M.Sc. Kaarlo Paakinaho for the PDLLA samples and the opportunity to take part into his research.

I would like to thank Dr. Alexander Efimov for taking care of providing always enough liquid nitrogen for my measurements. I give also my special thanks for all those who fetched it. I am grateful to Anne-Maarit Tikkanen for helping me to fill the nitrogen tank of the instrument and providing me all the laboratory equipment I needed. I thank also Dr. Mika Niskanen for the help in constructing the molecular models of PLA from the crystal structure data and Lecturer Raija Mikkonen for her advice about FTIR.

I would like to express my gratitude to my parents for their support and guidance for all of my life. My sister Jutta receive special thanks for having the same kind of sense of humor as I do. I really appreciate all the interesting conversations we have had. I thank all of my friends for their company, especially Sofia, with whom I have shared many happy moments. Finally, I wish to thank Mark for all these years. You and our little cat really know how to make my day, every day.

Tampere, 24th May, 2012

Tuuva Kastinen

CONTENTS

ABBREVIATIONS

ADSC	alternating differential scanning calorimetry
DSC	differential scanning calorimetry
DTA	differential thermal analysis
FTIR	Fourier transform infrared spectroscopy
PDLA	poly(D-lactic acid)
PDLLA	poly(D,L-lactic acid)
PEM	prediction-error method
PLA	poly(lactic acid), polylactide
P(L/D)LA 96/4	poly(L,D-lactic acid) with 96% L- and 4% D-content
P(L/D)LA 99/1	poly(L,D-lactic acid) with 99% L- and 1% D-content
PLLA	poly(L-lactic acid)
TMDSC	temperature modulated differential scanning calorimetry
TOPEM	advanced multi-frequency temperature modulated differential scanning calorimetry

SYMBOLS

$\%T$	percent transmittance
α	extent of reaction
A	absorbance
A_T	amplitude of the temperature modulation
β	underlying heating rate
c	concentration
C	heat capacity
C_p	heat capacity at constant pressure
c_{p0}	specific heat capacity; quasi-static heat capacity
$c'_{p,fi}$	in-phase heat capacity
$c''_{p,fi}$	out-of-phase heat capacity
$c^*_{p,fi}$	complex heat capacity
d	sample thickness
$f_{mod}(t)$	modulation function
ϕ	heat flow
ϕ_{non}	non-reversing heat flow
ϕ_{rev}	reversing heat flow
ϕ_{tot}	total heat flow
ΔG	free energy of fusion
ΔH	change of enthalpy
ΔH_c	heat of crystallization
Δh_i	specific enthalpy
ΔH_m	heat of fusion
ΔS	entropy of fusion
Δt	pulse width
$\delta T(t)$	stochastic temperature modulation
ΔU	change of inner energy
ε	molar absorption coefficient
$g(t)$	pulse response
I	intensity
λ	wavelength
q	heat; shift operator
t_{cw}	width of the calculation window
$u(T)$	input signal
$\bar{\upsilon}$	wavenumber
w	work
ω	angular frequency of the modulation
$X(\%)$	degree of crystallinity
$y(t)$	output signal

1 INTRODUCTION

Poly(lactic acid) (PLA) is an aliphatic polyester, which is composed of lactic acid. In the last decade, it has turned out to be a promising material in the industrial packaging field due to its biodegradability and safety for food contact. It is also used in medical applications. Properties of PLA can easily be altered by modifying its stereochemical structure and because of different ratio of L- and D-isomers the resulting polymer can either be semicrystalline or amorphous. [1; 2]

Even though PLA can be processed with standard equipment, its thermal behavior should be taken account, because different thermal conditions can result in different structures [1]. This is because of polymorphous nature of PLA, which means that it has several crystalline structures. Newly found α' form has attracted much attention, because it has been confirmed to be origin of the double melting behavior characteristic to PLA. [3; 4] Another noteworthy factor is the possible degradation of the polymer via hydrolysis, if certain thermal and humidity conditions are fulfilled [5]. For these reasons the properties of PLA should be examined closely [1].

Differential scanning calorimetry (DSC) is a common technique to study thermal properties of polymers [6]. Lately invented temperature modulated techniques (TMDSC) offer a new perspective to studies and they have found great favor alongside conventional DSC methods. The idea behind the TMDSC technique is to overlay a linear temperature ramp with a periodic waveform of small amplitude. [7] A commonly used waveform is a sine wave, but other temperature fluctuations, for example isothermal segment or sawtooth, are used as well [8; 9; 10]. The ability of TMDSC to distinguish the reversing processes from the non-reversing ones has simplified the interpretation of the curves, where these events usually are overlapped [7].

The latest TMDSC method is an advanced multi-frequency TMDSC technique, TOPEM [11]. In this method, the temperature fluctuations used are stochastic temperature pulses of different durations. A great advantage of this method compared to the previous ones is the possibility to perform one measurement over a large frequency range as a function of both time and temperature. This is done by using a prediction-error-method (PEM), which is a state-of-the-art mathematical method. The using of a broad band of frequencies eases the separation of frequency-dependent effects (e.g. glass transition) from frequency-independent ones (e.g. loss of moisture). Other advantage of this method is the possibility to determinate the quasi-static heat capacity. [12]

The measuring of melting processes by the TMDSC methods is a complicated task and in order to perform accurate analysis certain conditions should be fulfilled. It is pos-

sible to use TOPEM for analyzing the melting region, when the measurement program is chosen so that the linearity and stationary conditions of the measurement are satisfied. The suitable parameters are determined before the measurements in preliminary studies. When they are chosen correctly, TOPEM can provide valuable information about melting processes. [13]

In this thesis the double melting behavior of poly(L,D-lactic acid) (P(L/D)LA) with different D-contents (1 and 4%) was studied by TOPEM. The melting and crystallization properties of poly(L-lactic acid) (PLLA) have been studied widely with the conventional DSC method [3; 14; 15] and to some extent with TMDSC [16], but the presence and behavior of the α- and α'-forms in P(L/D)LA have been reported only for P(L/D)LA 98/2 [17] to the author's knowledge. Therefore, it is reasonable to study how the D-content affects this phenomenon. In addition, the performance of TOPEM in this region is examined, as well. The program parameters are selected based on the preliminary measurements. The results are compared to the ones obtained with the conventional DSC measurements. The results are also compared with the TMDSC data found in the literature.

Fourier transform infrared (FTIR) spectroscopy is another suitable instrument for examining the effect of different conditions on polymers. It is very sensitive to the changes in morphology and conformation of the sample. In addition, it is a nondestructive method, which enables using of the same sample for several times. [18]

Amorphous poly(D,L-lactic acid) (PDLLA) is one of the polymers, which have a water induced shape-memory. This phenomenon makes it very promising material in medical devices. The shape-memory of PDLLA is activated by the plasticizing effect of water. [19] So far it has been unclear, how water molecules interact with this polymer. There have been many studies about the influence of water on hydrophilic polymers, but for some reason hydrophobic polymers, especially PLA, has not been as widely studied [20]. The plasticizing effect of water on PDLLA was examined by FTIR in the other part of this thesis. In addition, the effect of gamma sterilization was studied and the results of unsterilized and sterilized samples were compared.

2 THERMOPHYSICAL PROPERTIES OF POLYMERS

In thermodynamics a system refers to a unity of the all materials related to the process concerned. The surroundings in turn include the rest of the universe. [21, p. 2] The first law of the thermodynamics states that in the isolated system the inner energy of the system, U, is constant. In other words, the energy cannot be created or destroyed. Thus, $U_{\text{surroundings}}$ must decrease by the same amount as U_{system} increases. The only manner to influence the inner energy is to alter work, w, or heat, q, flowing across the boundary between the system and the surroundings. When they are summed up, the resulting function corresponds to the following formulation of the first law [21, pp. 13–14]:

$$\Delta U = q + w. \tag{2.1}$$

Work can be defined here as energy that is used to change the state of the system by changing the volume of the system. When w is positive, the surroundings do work on the system and vice versa in the case of negative w. Heat is the amount of energy flowing across the boundary due to the temperature difference between the system and the surroundings. The heat flow is directed from the surroundings to the system, when q is positive and the other way around when q is negative. [6, p. 132; 21, pp. 14–17]

The internal energy that is either released or absorbed during chemical and physical transformations is referred as enthalpy, H. At the constant pressure it can be written

$$H = U + PV, \tag{2.2}$$

where P is the external pressure applied to the system and V is the volume of the system. The change of enthalpy, ΔH, between two states is one of the main quantities measured by calorimetric methods. Endothermic processes increase ΔH of a sample, while exothermic reactions decrease it, respectively. [6, p. 132; 22, pp. 36–37]

2.1 Heat capacity

The heat capacity is a very important material-dependent property that is defined as the amount of heat, which is required to raise the temperature of a sample by a certain amount, dT [21, p. 19; 23, p. 90]

$$C = \frac{q}{dT}. \tag{2.3}$$

The experimental conditions affect the value of the heat capacity [21, pp. 20]. In an adiabatic calorimeter processes occur at constant pressure, in which case the heat capacity can be expressed as the partial derivate of the enthalpy with respect to the temperature [11, p. 101]:

$$C_{\mathrm{p}} = \left(\frac{\partial H}{\partial T}\right)_{\mathrm{p,n}}. \tag{2.4}$$

The units of the heat capacity are given per gram (J K^{-1} g^{-1}) or per mole (J K^{-1} mol^{-1}). The specific heat capacity refers to the heat required to raise the temperature of the one gram sample by 1 K (or 1 °C), while the molar heat capacity is the heat capacity of one mole of the sample. [24]

2.2 Glass transition

When an amorphous or semicrystalline polymer is heated past a certain temperature it undergoes the glass transition, during which it transforms from a rigid solid to a rubbery material and further to a liquid. The process is reverse, when a liquid is cooled to a solid. [25, p. 545; 26, p. 119] In this case, however, the glass transition occurs only if the cooling rate is fast enough, otherwise a polymer may crystallize [27, p. 164]. The glass transition temperature, T_{g}, refers to the temperature at which half of the transition has occurred [23, p.118]. In other words, at this point a rigid glass softens and transforms to an elastomeric material [25, p. 546; 26, p. 119]. Because neither glassy nor the viscous state is in equilibrium, the glass transition cannot be classified as a first- or second-order thermodynamic phase transition. However, since it resembles so much a second-order phase transition the glass transition is termed a pseudo second-order transition. [23, p. 116]

At T_{g} many physical properties of polymers have been observed to change suddenly, namely elastic modulus, heat capacity, expansion coefficient and specific volume [22, p. 44; 26, p. 119], which is plotted against temperature in Figure 2.1. A discontinuity in the curve is observed for both totally amorphous (upper curve) and semicrystalline polymer (middle curve), whereas for the totally crystalline polymers, the curve would be straight line (lower curve). There are no disordered chains in the totally crystalline polymers, due to which no glass transition is observed for them. Melting of the crystalline polymer would occur at T_{m}^{0}, which is an equilibrium melting point. This is however just theoretical assumption, because there is no polymer produced with 100% crystallinity and thus melting of the semicrystalline polymers is always observed at lower temperatures (T_{m}). [25, p. 546; 28, p. 14]

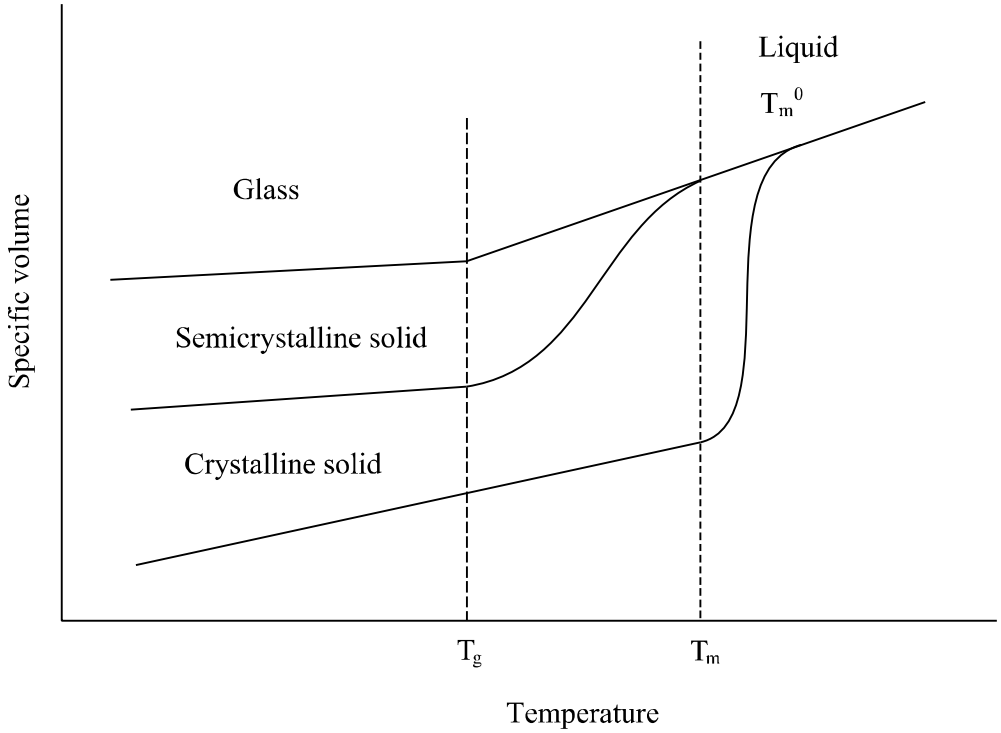

Figure 2.1 *Determination of the glass transition (T_g) and the crystalline melting temperatures (T_m) is presented by expressing specific volume against temperature for the totally amorphous (upper curve), semicrystalline (middle curve), and crystalline (lower curve) polymer. Melting of the totally crystalline polymer occurs at the equilibrium melting point (T_m^0). Adapted from [25, p. 546; 28, p. 14]*

There are many factors that have an influence on T_g, for example the configuration of the polymer, the degree of crystallinity, and the length of the side groups [26, p. 119]. The size and structure of side groups affect chain flexibility and its ability to rotate. The larger the side group, the more it limits chain rotation and increases T_g. Double bonds, polar, and aromatic groups located in the backbone of polymer have the similar effect. [25, pp. 547–548]

2.3 Crystallization

Polymers, which have a sufficiently ordered structure, are capable to organize into regular crystalline structure, when they are slowly cooled from their molten states or hot solutions [26, p. 24; 27, p. 158]. This process is called crystallization and it occurs through nucleation and growth processes [25, p. 544; 27, p. 159]. When crystallization is incomplete, semicrystalline structure, containing both amorphous and crystalline regions, is formed. The fraction of crystalline region is described by the degree of crystallinity. Crystallization temperature in turn is the point at which crystallization starts when cooling from the melt. [26, pp. 24, 121]

At the beginning of the crystallization, nuclei of the new phase start to appear in the initial one. These particles are capable of growing, when an embryo surpasses the critical size and becomes stable. Nucleation can be either homogeneous or heterogeneous

depending on the point, where it occurs. In the case of homogeneous nucleation, nuclei form in every part of the initial phase, whereas for the heterogeneous nucleation it occurs mainly at structural inhomogeneities that can for example be surfaces, impurities or grain boundaries. When an embryo has reached the critical size and stabilized, the growth process begins, while nucleation continues simultaneously.
[25, pp. 313, 320]

Chains organize into lamellar structure, which is in the most of cases the extended chain or planar zigzag conformation. When a polymer has larger substituent groups, the preferred conformation is a helix. Some polymers tend to organize into spherical structures, which are termed spherulites. These kinds of structures are composed of lamellar crystallites, whose orientation is usually perpendicular to the radial growth direction of the spherulite. [27, p. 159]

2.4 Crystalline melting temperature

The melting of a polymer is a physical process in which a solid material transforms to a liquid, while its structure changes from ordered to a random one. This process is characterized by the melting temperature, T_m, at which the curve of a crystalline material has a discontinuity (Figure 2.1). [25, p. 545] It is usually used for purity determination, identification of a substance, and calibration of thermometers and other instruments [22, p. 63].

The free energy of fusion per a repeating unit of polymer, ΔG_u, is expressed by using the first law of thermodynamics:

$$\Delta G_u = \Delta H_u - T\Delta S_u, \tag{2.5}$$

where ΔH_u is the enthalpy of fusion and ΔS_u is the entropy of fusion per repeating unit. The free energy is zero at the equilibrium temperature ($T=T_m^0$), which leads to

$$T_m^0 = \frac{\Delta H_u}{\Delta S_u}. \tag{2.6}$$

The crystalline-melting temperature observed always differs from the theoretical one. [27, p. 162] Only pure substances have a single melting point, while polymers have a range of temperatures [22, p. 63].

Structural factors affecting the melting temperature are similar to those described for T_g in subsection (2.2) Molecular weight[1] of polymer has also a connection with the magnitude of T_m, for increasing it raises T_m, respectively. [25, p. 547] On the contrary, the presence of a plasticizer can reduce T_m [27, p. 159]. As stated above, crystalline

[1] In this case, molecular mass, molar mass, and relative molecular mass would be more appropriate terms than molecular weight. However, it is commonly used in the literature and thus will be used in this thesis as well.

polymers do not have a single melting temperature. This is because of the presence of impurities and molecules with different molecular weights and sizes [25, p. 547]. Smaller crystals melt faster than larger and more perfect ones [29, p. 46]. Other affecting factor is possible polymorphism of a polymer, which means that it exists as a mixture of several crystal modifications [22, p. 62].

3 POLY(LACTIC ACID)

Poly(lactic acid) has several names. It is also called polylactide or poly(2-hydroxy propanoic acid), the latter being its systematic IUPAC name. PLA is a rigid thermoplastic polymer, which belongs to the family of aliphatic polyesters. It can be produced from renewable resources. Moreover, it is biodegradable and when it has been properly disposed of, it will degrade to harmless products, which decompose within two years. Due these reasons the polymer has aroused lots of attention lately and its properties have been widely studied. The commercial use of poly(lactic acid) is centred in packaging industry and medical applications. [2]

High-molecular-weight PLA is colorless, glossy, and rigid by structure. Due to the chirality of its building block, lactic acid, PLA has several different compositions. Poly(L-lactic acid) (PLLA) and poly(D-lactic acid) (PDLA) are both optically pure, semicrystalline polymers with similar thermal properties. [30, pp. 538–539] Poly(D, L-lactic acid) (PDLLA), in turn, is amorphous by structure due to randomly alternating L- and D-lactic acid sequences. Ratio of two enantiomers has a great effect on the properties of the polymer, including thermal properties and degradation. [31, p. 113]

PLA is polymorphic material, which means that it has more than one crystalline structure. Recently found α' form has been the center of attention, because it is found to be a reason for multiple melting behavior characteristic to the polymer. [3]

3.1 Structure

The basic building block of poly(lactic acid) is 2-hydroxypropanoic acid (systematic, IUPAC name), which is also called lactic acid (common name). It has, due to a chiral carbon atom, two enantiomeric forms, termed (2*S*)-2-hydroxypropanoic acid and (2*R*)-2-hydroxypropanoic acid or (*S*)- and (*R*)-lactic acid, respectively (Figure 3.1). [32, pp. 3–4] Humans and other mammals produce (*S*)-lactic acid, while both forms appear in bacterial systems [2]. Other method to name enantiomers of a chiral molecule is to use the labels L (for laevo) and D (for dextro). This is an arbitrary convention according to which two enantiomers of glyceraldehyde were named. Glyceraldehyde was used as a standard against which other compounds were compared. Nowadays, this naming practice is used only for certain, well known molecules, in whose case it is justified due to the tradition. [33, p. 389] In the literature the enantiomers of lactic acid are commonly described as L- and D-lactic acid, and hence this practice is applied in this thesis, as well.

L-lactic acid D-lactic acid

Figure 3.1 *Structure of (S)- and (R)-lactic acid, which are usually referred as L- and D-lactic acid, respectively [32, p. 4].*

Step-growth polymerization of lactic acid leads to a low-molecular-weight polymer, which is brittle and glassy by structure. Depolymerization of this polymer leads to cyclic dimer termed 3,6-dimethyl-1,4-dioxane-2,5-dione (systematic, IUPAC name) or lactide (common name), whose three different structures are shown in Figure 3.2.

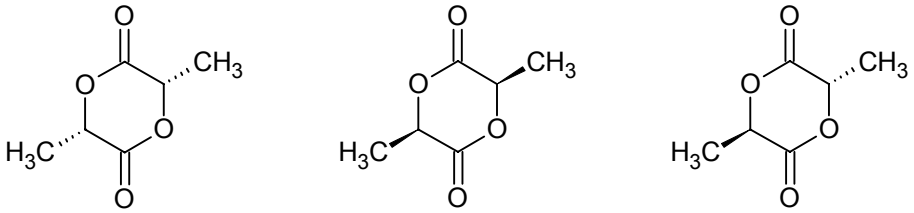

L-lactide D-lactide *meso*-lactide

Figure 3.2 *The three diastereomeric structures of lactide [32, p. 11].*

Lactide can be L-lactide, D-lactide, or *meso*-lactide (DL-lactide), depending on the enantiomer of lactic acid used. Fourth existing structure is a racemic mixture of L-lactide and D-lactide, which is termed *rac*-lactide. [32, p. 11] Lactide is polymerized further by ring-opening polymerization (ROP) to the high-molecular-weight PLA [2]. A more detailed synthetic route is illustrated in the next subsection (3.2).

The structural formula of PLA is shown in Figure 3.3. The polymer is either amorphous or semicrystalline depending on the ratio of two enantiomers. When L-lactic acid is polymerized the resulting polymer is poly(L-lactic acid) (PLLA). Polymerization of D-lactic acid, in turn, leads to poly(D-lactic acid) (PDLA). Both polymers have same kind of properties, such as optical purity and semicrystalline structure. However, the properties of PLLA have been more widely investigated, because the building block of the polymer, L-lactic acid, can be easily produced from renewable resources by fermentation of sugars from carbohydrate sources (corn, sugarcane, or tapioca) with suitable microorganisms. The production of D-lactic by this manner is far more difficult, although several natural D-enantiomer producing bacteria are known. [32, pp. 3, 6–7]

An atactic copolymer referred as poly(*meso*-lactide) is formed when *meso*-lactide is used as a starting material. Using of equimolar amounts of L- and D-lactide yields to random optical copolymers termed poly(D, L-lactic acid) (PDLLA, 50% D and 50% L)

or poly(*rac*-lactide), whose structure is also atactic but segregated into optical doublets of the lactyl group. Both poly(*meso*-lactide) and PDLLA are amorphous. [30, p. 539] Because there are always some *meso*-lactide impurities present in the production processes of PLA, commercial polymers are actually copolymers containing both L- and D, L-lactide [34].

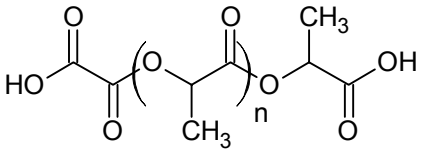

Figure 3.3 *The structural formula of poly(lactic acid) [2].*

PLLA has four different crystal structures depending on preparation methods and treatment conditions. The most general structure is the α form that is formed as a result of melt or cold crystallization, and solution spinning processes, when using low draw ratios and/or low temperatures. The α form is proposed to have a 10^3 helical structure with two antiparallel chains, which are in an orthorhombic unit cell. [35] However, recently Wasanasuk et al. discerned that erasing of the 2_1 screw symmetry along the molecular chain results in the crystal structure with higher accuracy [36]. The new model is illustrated in Figure 3.4 alongside the most recently found α' form, which has attracted much attention lately because it has been noticed to be a source to a multiple melting phenomenon of PLLA. The α' form has the same kind of structure as the α form but its side groups are noted to be less ordered and looser. [4] Thus, it has the disordered 10^3 helical conformation. According to Wasanasuk et al. it is a completely different crystalline form than the α form. They suggested two models, the most probable one of which consists of alternating upward and downward chains with relatively high disorder. For avoiding the confusion between the α and α' forms they suggested a new name for the latter, namely the δ form. [37] However, in this study the name "α' form" is still used.

The β form can be found in the poly(L-lactic acid) fibers. It has a so-called frustrated structure, which consist of three 3_1 helices packed in a trigonal unit cell. [38] The β form can be formed from the α form by stretching at a high draw ratio. This transition has been noticed to occur through the α' form. [37] Another possible preparation method is solution spinning using high draw ratios and temperatures.

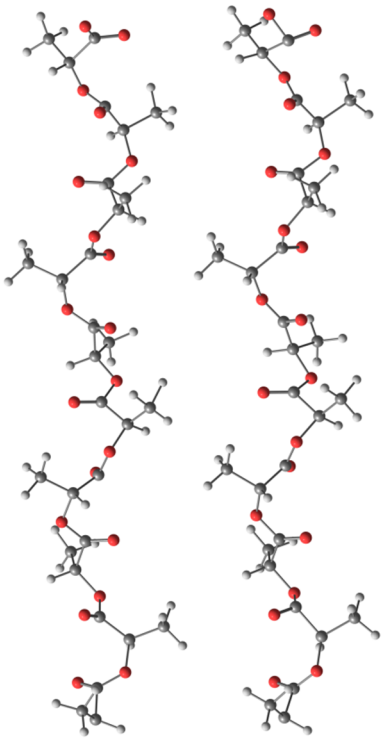

Figure 3.4 *The crystal structures of the α (left) and α' forms (right) suggested by Wasanasuk et al [36; 37].*

The melting temperature of β form is lower than the one of the α form, while the latter is the more stable structure. [39] The fourth form, γ, is prepared by the epitaxial crystallization. It has two antiparallel 3_1 helices in an orthorhombic unit cell [40].

3.2 Processing

Poly(lactic acid) can be produced directly from lactic acid by step-growth polymerization. Old term, which is still commonly used in literature, is condensation polymerization. This, however, leads to a low-molecular-weight PLA, which is glassy and brittle by its structure. Commercially more effective routes are depicted in Figure 3.5. Through them, it is possible to produce the high-molecular-weight polymer in a high yield. [2; 32, p. 3]

Route 1 illustrates the direct step-growth polymerization of lactic acid, during which water is condensed out. This is the least expensive method, but it requires the usage of coupling agents, which usually complicates the process and raises costs. The first stage of polymerization is polymerization of lactic acid to the low-molecular-weight prepolymer. It has both the hydroxyl and the carboxyl end-groups that react with coupling agents. Unfortunately, some of them might remain unreacted in the final product alongside the other impurities. Coupling agents normally used are anhydrides, epoxides, and isocyanates. Another possibility is to use esterification-promoting agents, like bis(trichloromethyl) carbonate, *N,N'*-dicyclohexylcarbodiimide, and 1,1'-carbonyldiimidazole, which makes the final polymer pure and free from used catalysts or oligo-

mers. This process involves however high number of steps and requires removing of the remaining by-products. [2]

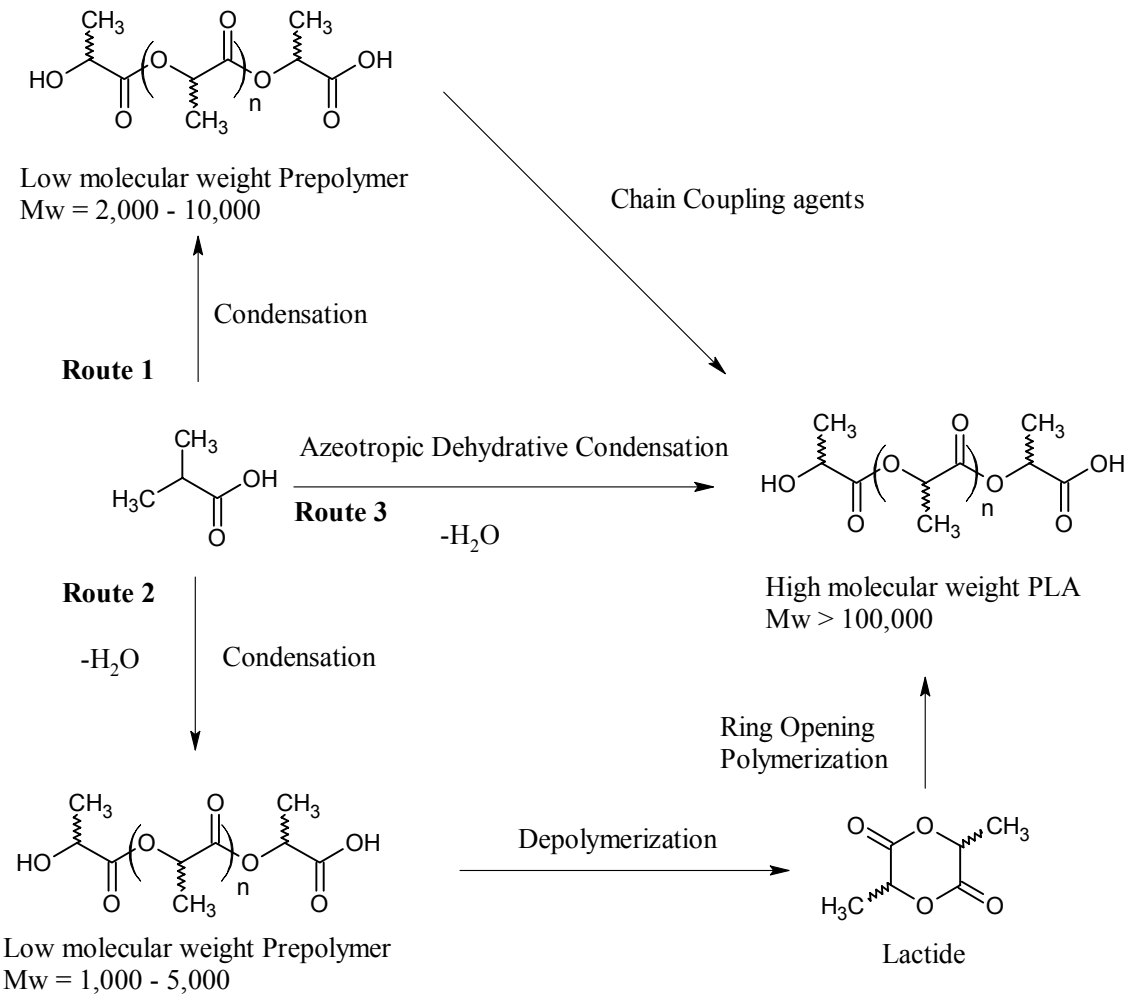

Figure 3.5 *Production routes of poly(lactic acid) with different molecular weights [41].*

Another method to produce the high-molecular-weight PLA is polymerization through intermediate product, lactide, the cyclic dimer of lactic acid (Route 2). This method patented by Cargill Inc. is nowadays the mostly used process, in which depolymerization of two low-molecular-weight poly(lactic acids) yield L-lactide, D-lactide or *meso*-lactide. The mechanism of the formation of lactide ring is presented in Figure 3.6. The final product is obtained from lactide by ring-opening polymerization, which can be either cationic or anionic. [2; 41]

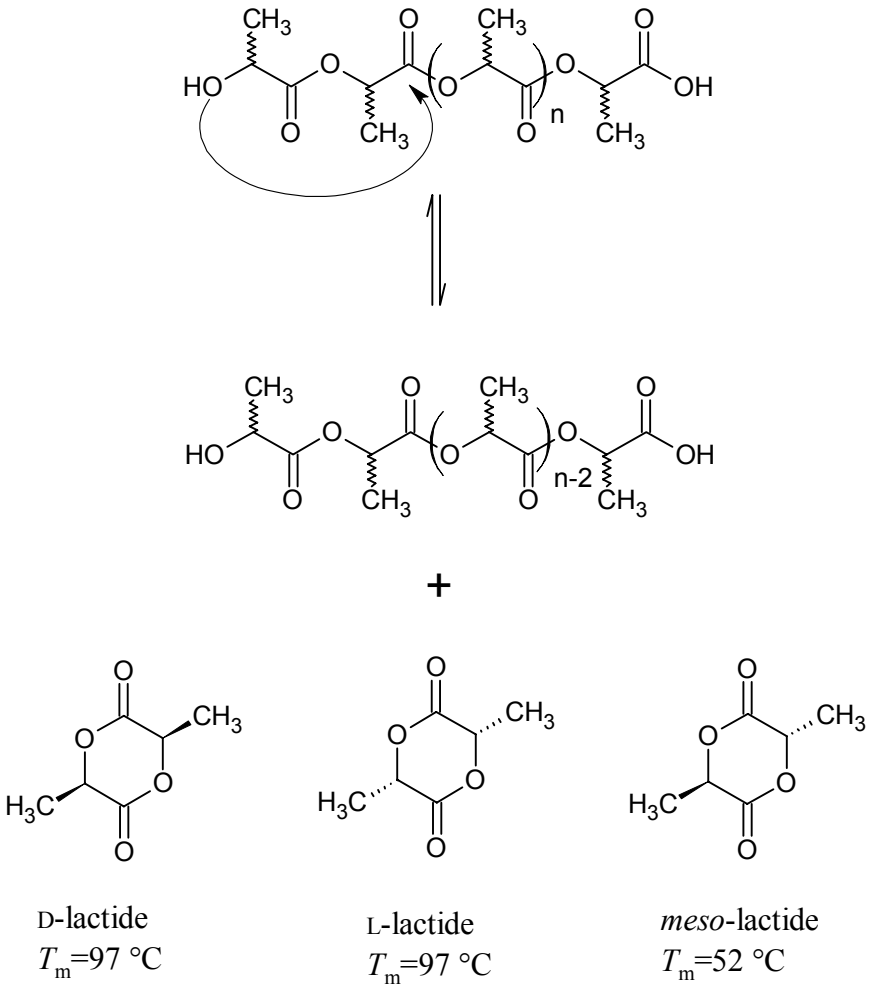

D-lactide
T_m=97 °C

L-lactide
T_m=97 °C

meso-lactide
T_m=52 °C

Figure 3.6 *Formation of D-, L-, and meso-lactide from the low-molecular weight pre-polymer [41].*

The solvent is either dried from the water with a drying agent or chosen amongst dry organic solvents, which, however, is not so of an ecological option. When diphenyl ether is used as a solvent, the most effective catalysts have been reported to be tin compounds, nickel diacetate ($Ni(OAc)_2$), and methylbenzenesulfonic acid (CH_3-Ph-SO_3H). [42, p. 32] Due to high concentration of catalysts needed some residues remains, which can affect the process by leading up to degradation or hydrolysis [43, p. 437].

3.3 Thermal properties

The glass transition temperature defines the upper temperature, at which amorphous PLA can be commercially used. For semicrystalline polymer, the melting temperature is another determining factor. [30, pp. 538] At the temperatures lower than T_g PLA is in glassy state, while at higher temperatures it is rubbery by its structure. Compared to other thermoplastics the glass transition temperatures of PLA are relatively high, while its melting temperatures, in turn, are lower. The optical purity of the polymer affects the magnitude of T_g, for the higher content of D-lactide decreases it. Another influencing

factor is molecular weight. Polymers with higher molecular weight have higher T_g. The thermal history of PLA should be also taken into account. Rapid cooling of the molten polymer, for example, will lead to the amorphous structure. [1]

Similarly, the optical purity determines the magnitude of the melting temperature of PLA. Both pure PLLA and PDLA have T_m around 180 °C [1] and the equilibrium melting temperature around 207 °C [2]. Lower L-content leads to lower melting temperatures. The dependence of the T_m on molecular weight is similar as for T_g. Elevated molecular weights lead to higher T_m values. [1] The effect of the ratio of L- and D-content can be seen in Table 3.1, where the glass transition and the melting temperatures of different PLA polymers are expressed.

Table 3.1 *The glass transition and melting temperatures of pure PLLA and PDLA, fully amorphous PDLLA, and PLA with decreasing L-content [44].*

Polymer	T_g **(°C)**	T_m **(°C)**
PLLA	61.2	178.3
PLA(95)	60.0	150.7
PLA(90)	58.4	132.4
PLA(85)	57.0	-
PLA(80)	54.8	-
PLA(75)	53.4	-
PDLLA	50.4	-
PDLA	61.1	182.0

As stated before, PLA can be either amorphous or semicrystalline. Depending on the optical purity and the treatment conditions the polymer can be crystallized from melt. Slow cooling rates are required to result in the polymer with high crystallinity. In addition, L-content should be greater than 90%, otherwise the resulting structure will be amorphous. [1] The degree of crystallinity can be calculated from

$$X\ (\%) = \frac{\Delta H_m - \Delta H_c}{93.1} \cdot 100, \tag{3.1}$$

where ΔH_m is the heat of fusion and ΔH_c is the heat of crystallization obtained by DSC [30, p. 551]. The value of the enthalpy of fusion of 100% crystalline PLLA and PDLA polymers is 93.1 J g^{-1} [45]. The molecular weight and presence of nucleation agents have also an influence on the crystallization process of PLA [1; 30, p. 552]. For example talc has shown to be very effective nucleation agent because it reduces the half-time of crystallization [46].

3.4 Multiple melting behavior

Multiple melting behavior has been observed for several semicrystalline polymers [47], including poly(ethylene terephthalate) (PET) [48], poly(butylene terephthalate) (PBT) [49], and poly(trimethylene terephthalate) [50]. In the case of PLA this phenomenon occurs as two endotherms accompanied by a small exotherm at certain temperatures [3]. Many authors have investigated the provenance of the double melting peaks and different explanations have been proposed. The most popular one has been a melt-recrystallization model [47 p. 133; 51; 52], according to which the endotherms originate from the melting of the original crystals and the crystals formed during the melt-recrystallization. An exotherm between the peaks is associated with recrystallization. [47, p. 133]

Other explanations have been dual (or multiple) lamellae population, dual (or multiple) crystal structure or the existence of different crystal structures [15; 51]. The dual lamellae population mechanism was first proposed by Cebe and Hong [53] and Bassett et al [54]. It states that lamellae with different thicknesses form during DSC experiment. The low-temperature endotherm is due to the melting of the thinner lamellae and the high-temperature endotherm originates from the thicker lamellae, respectively. [55] Polymorphism of the polymer or the presence of the different crystal structures can also result in the double melting peaks [15].

PLA is known to crystallize as the α form, when the crystallization temperature (T_c) is over 120 °C. Below 90 °C, is the recently found α' form the dominant one and DSC curve is characterized with a small exotherm prior to the single melting peak. [14] The exotherm has been confirmed to correspond to a disorder-to-order (α'-to-α) phase transition by Zhang et al. It disappears above 110 °C, while second melting peak appears before the first one. At first it is significantly smaller than the dominant melting peak, but its temperature and magnitude increase with increasing crystallization temperature. Simultaneously the first peak gets smaller and eventually disappears. [3] At $T_c \geq 110$ °C, Shen et al. observed also a third endotherm prior to the two endotherms, when studying the crystal modifications and multiple melting behavior of poly(L-lactic acid-*co*-D-lactic acid) (98/2) [17].

There have been some suggestions concerning the possible mechanism of the disorder-to-order phase transition. Kawai et al. proposed that the transition occurs at 150 °C without melting that is through the solid-solid phase transition. They justified this assumption by an observation that the peak temperatures and shapes of the crystallization and the melting peaks stay almost unchanged with the varying heating rate. [14] On the contrary to that, Shen et al. noticed that the presence of the second melting peak before the exotherm in the DSC curve of the α' form depends strongly on the heating rate, which suggest that a melting process involves in the phase transition. They stated also that the rate of the phase transition increases with increasing temperature. [17] According to Zhang et al. the α'-to-α phase transition is the first-order transition. At lower temperatures the size of the α' crystallite increases with increasing T_c.. The α crystallite

starts to appear above 100 °C and the domain size of the α form gets larger, while the α' domain decreases. During the phase transition the lattice spacing of both forms decreases, which refers to more compacted packing of them. [3] Recently Wasanasuk and Tashiro came up with similar conclusions when investigating the phase transition mechanism by X-ray diffraction. The transition from the α' to α form was observed to occur discontinuously at around 120 °C. Increasing temperature activates the thermal motion of the chains, which regularizes their conformation and tightens the chain packing of the domains. The relative height of the domains is adjusted when the small regions move along the chain axis and finally merge into larger, more regular domains. These domains start to transform to the α form and for some time both forms coexist in the polymer. More domains transform to the α form with increasing temperature and finally, when the temperature gets high enough, a single domain should be formed from larger α domains. However, some regions with disorder coexist still, because transformation is not completely ideal. [37]

Origin of the double endotherms for PLLA has been studied by many authors. Lorenzo suggested that the peak at lower temperature (P_2) is due to fusion of crystals that have a low thermal stability and are formed at T_c or T_{exo}. Structural reorganization leads to the perfected crystals that melt at higher temperature (P1). [52] More detailed definition was given by Pan et al. According to them the peak at lower temperature (P_2) is associated both with the phase transition and the melting of the original α form crystals, while the endotherm at higher temperature (P_1) arises from the α form formed during the phase transition and melt-recrystallization process. [15] The double-melting behavior has also been observed for PLA copolymers. As mentioned before, Shen et al. used poly(L-lactic acid-*co*-D-lactic acid) (98/2) in their studies. They explained the multiple-melting peaks to originate from lamellae with different thicknesses. The P_2 is due to the melting of the primary lamellae, while P_1 arises from the remelting of reorganized lamellae during heating. The third endotherm (P_3) was explained with the thinner lamellae located in the excluded regions. The α form undergoes the melt-recrystallization mechanism, while α' form undergoes simultaneously both melting and the phase transition. [17]

Alongside the crystallization temperature, the crystallization time is known to also affect the shape of DSC curves. With longer crystallization time more perfect crystals are formed, which influences the melting process. Lorenzo did not however find significant changes in the melting peaks with the crystallization times between 10 and 60 minutes. [52] Other affecting factors are the heating and cooling rates. Yasuniwa et al. discerned that the curves change significantly with the changing heating rates. Double-melting peaks are present in the curve when using the heating rate between 0.5 and 10 °C min^{-1}. With an increasing heating rate the area of the peak P_2 increases while the peak P_1 decreases. According to the melt-recrystallization model, this is due to competition of the melting and recrystallization processes during heating. An endotherm appears, when the rate of recrystallization process is slower than that of melting. In other words, recrystallization is overwhelmed by melting when using higher heating rates.

The effect of the cooling rate on the peaks is completely opposite. The region, where the double peaks are observed, is narrower than that in the case of the heating rate, namely 0.7–3 °C min^{-1}. [56]

Pan et al. investigated the effect of molecular weight on the multiple melting behavior of PLLA by both DSC and FTIR. They concluded that it has no influence on polymorphism. However, crystallization kinetics and rate were noticed to change with the changing molecular weight. Increasing molecular weight shifts the crystallization peaks to lower temperatures and broadens the peaks. At low crystallization temperatures the α'- to α-crystalline phase transition occurs in both the high- and low-molecular-weight PLLA. In the low-molecular-weight PLLA all the α' form crystals do not transform and some of them melt during heating, while in high-molecular weight PLLA the phase-transformation is more complete. [15]

3.5 Effect of water

Poly(lactic acid) is known to degrade, when it is exposed to high temperatures or humid conditions. This process is dependent on molecular weight and the crystallinity of the polymer. [5] Hydrophobicity and semicrystalline structure of a polymer restrain fast penetration of water. When the polymer contains some fraction of amorphous phase, diffusion of water is focused on these areas. At temperatures lower than T_g, water causes the chain segmental motion to increase, which is called the plasticizing effect of the diffused water. When the chain length becomes short enough, it enables the original amorphous region to rearrange in crystalline domains, which increases crystallinity. At higher temperatures, hydrolysis of ester bonds of PLA occur, which is also centred in the amorphous region of the polymer. The lactic acid oligomers formed in this reaction catalyze the process further. Implant industry take the effect of water very seriously, because it may cause implants to fail prematurely. [5; 42, p. 121]

However, the plasticizing effect of water can also be exploited, when one wants to change the shape of the polymer in a controlled way. For example amorphous PDLLA has a water induced shape-memory, which makes it very promising material in medical devices. [19]

Degradation of PLA caused by water occurs via hydrolysis (Figure 3.7), whose kinetics is controlled by its rate constant, water concentration, temperature, and morphology of the polymer. The presence of acids or bases increases the rate of hydrolysis. It is also observed to be much greater above the glass transition temperature than below it. Prevention of hydrolysis is not easily done, because PLA is quite permeable to water and the reaction is autocatalyzed. Some possible methods are reduction of the number of remaining monomers, lowering of the water concentration, and prevention of autocatalysis. At pH 7.4 and temperature of 37 °C, bulk hydrolysis is observed to occur faster compared to surface hydrolysis. This is because of the autocatalysis caused by the carboxylic acid end groups, which are produced during the hydrolysis process. As stated

before, water can penetrate the amorphous regions of polymer, but not the ones, which undergo hydrolysis mainly through surface erosion. [30, pp. 556–559]

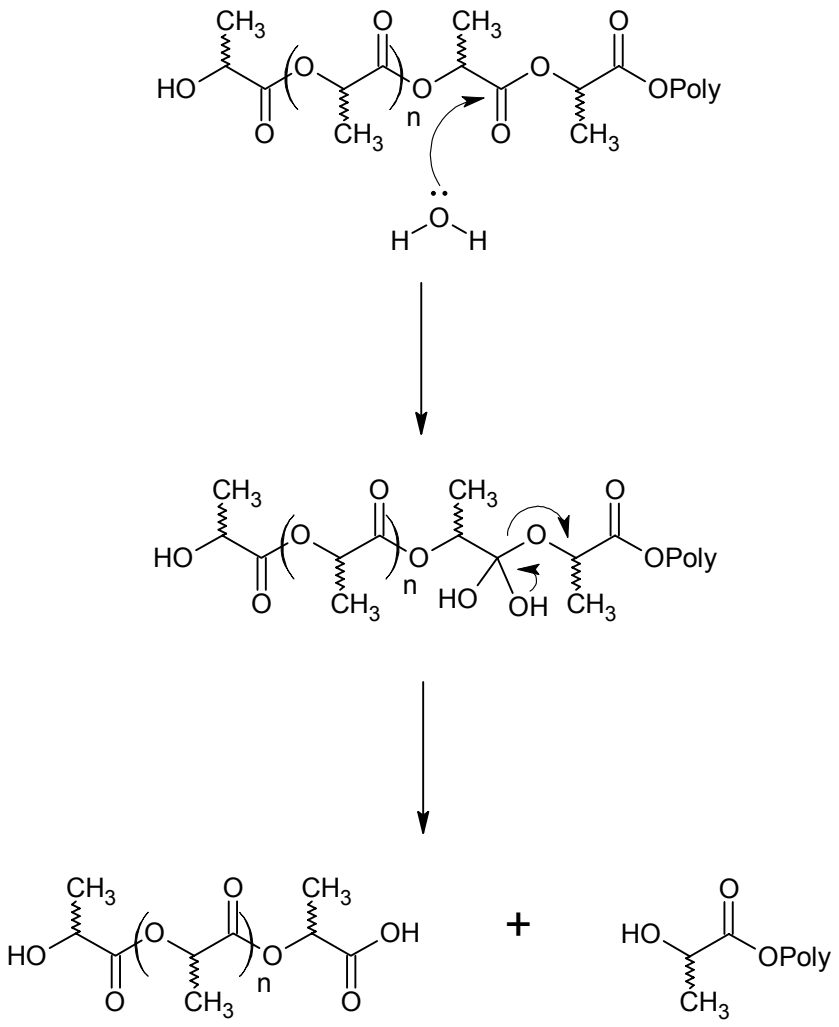

Figure 3.7 *Degradation of PLA via hydrolysis reaction caused by water [41].*

There have been reported to be three kinds of water interacting with hydrophilic polymers. Non-freezable bound water is closely associated with the polymer matrix and it cannot be seen with calorimetric analysis. The freezable bound water is the further-most water fraction from the matrix and its melting and crystallization differ so much from bulk water that those two can be separated. Temperature events of freezable free (bulk) water are almost the same as observed for bulk water. [20]

So far, it has been unclear, how water molecules interact with this polymer. There have been many studies about the influence of water on hydrophilic polymers, but for some reason hydrophobic polymers, especially PLA, has not been as widely studied. Blasi et al. investigated plasticizing effect of water on poly(lactide-co-glycolide). They came to the conclusion that non-freezable water is the influencing factor on this process. [20]

4 DIFFERENTIAL SCANNING CALORIMETRY

The history of the differential scanning calorimetry (DSC) begins in principle already in the middle of the 19th century, when calorimetry and heating curves were developed. After invention of automatic and continuous monitoring of temperature with thermocouples, differential thermal analysis (DTA) was publicized. Le Chatelier was the first one to use the principle behind the technique, but the first full DTA measurement was performed at the beginning of the 20th century. Until 1950s DTA was used only for determination of phase transitions and chemical reactions. When the recording system was updated with electronics, quantitative analysis became possible and the instrument was called DSC. Further development of technique enabled the direct connection between the apparatus and a computer. Nowadays DSC is in common use in many scientific fields. The development of technique is lately focused in upgrades of softwares, which can be seen in invention of temperature-modulated DSC and the most recently TOPEM, which is the advanced multi-frequency TMDSC technique. [11, pp. 329–331]

In summary, DSC is a technique in which temperatures of a sample and a reference are continuously controlled by a temperature program, while a difference between energy supplied to them is analyzed. The conventional DSC method is used to analyze different thermal properties of several materials, for example polymers, glasses, metals, and oils. The most commonly performed measurements are related to thermal transitions of polymers, namely glass transition, crystallization, and melting. [6, pp. 57, 60]

4.1 Instrument

Depending on the operating principle of DSC, the commercial instruments can be classified as either heat flux or power compensation DSCs (Figure 4.1). The apparatus used in this study, Mettler Toledo DSC1, belongs to the first class. In this type of DSC both the sample and the reference are located in the same furnace. The temperature difference between them is measured by sensors and converted to the heat flow, Samples are inserted into small crucibles, which are, depending on the type of instrument, placed on a disk or in hollow cylinders. An empty crucible is usually used as a reference. The principle of DTA is very much the same. [6, p. 58; 23, p. 16; 57, p. 5]

In the disk-type DSC temperature sensors are integrated in the disk or they contact the disk surface. In ideal situation the temperature difference between the sample and the reference, ΔT, is zero, while heat flows through the disk to them. If a transition occurs in the sample, ΔT is altered. This change is proportional to the difference between the heat flow rates directed to the sample and the reference. The furnace of the cylinder-type DSC has two or more cylinders located in cylindrical holes. Samples can be placed

in the bottoms of them with or without crucibles. The cylinders are connected to the furnace with thermopiles or thermoelectrical semi-conducting sensors, which measure the temperature difference between two cylinders. [23, p. 17]

In the case of a power compensation DSC the sample and the reference are placed in two separate furnaces, both of them equipped with an own heating unit and a temperature sensor. The two furnaces are heated separately, while the temperature difference between them is kept in minimum by controlling the heating power directed in the sample and the reference. When a reaction occurs in the sample, the difference in the heat flow rates between the sample and the reference can be assumed to be proportional to this power. [23, p. 18]

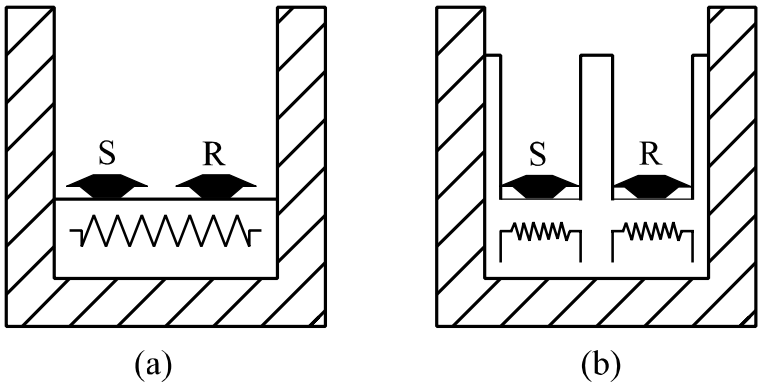

Figure 4.1 *Schematic representation of (a) heat-flux DSC and (b) power compensation DSC. Adapted from [6; 58].*

The power compensation DSC can attain higher heating and cooling rates compared to the heat flux DSC [57, p. 7]. However, its operating temperature range is usually narrower [58, p. 57]. The temperature range for DSC1 is from -150 to 700 °C when using liquid nitrogen cooling. Other possible cooling systems are air cooling, cryostat cooling, and IntraCooler. The heating rates of the DSC1 instrument are between 0.02 and 300 °C min^{-1} and the cooling rates are 0.02–50 °C min^{-1}. [59] DSC measurements are in most cases carried out in an inert atmosphere, which means that purge gas, usually nitrogen, is directed to the measuring chamber. It flushes out both air and gaseous products originating from the sample with a specified flow rate. [22] Another inert gas used is helium. It is also possible to carry out measurements under air or oxygen atmosphere. [60, p. 26] Calibration of a DSC instrument is performed by using standards, whose transition temperatures are well known. The most used method is determination of the melting point of pure metals, namely indium and zinc [60, pp. 26–28].

4.2 Conventional DSC

In a conventional DSC measurement the difference in the heat flow between the sample and the reference, dq/dt is plotted against time, t, or temperature, T. The resulting curve can be divided in different sections, namely baseline, steps, and peaks. [23, p. 37] When

the reaction is endothermic, for example melting, a sample receives heat from surroundings. This can be seen as a decreased heat flow rate in the DSC curve. In the case of exothermic reactions this is the opposite. [21, p. 64] The glass transition in turn shows as a step in the graph [23, p. 39]. The heat flow depends on the heat capacity of the sample in the following way [57]:

$$\frac{dq}{dt} = C_p \cdot \frac{dT}{dt}. \tag{4.1}$$

The area limited by the peak and the interpolated baseline, that is, peak area is related to the enthalpy change resulting from the thermal event. As stated above, the *dq/dt* is plotted against *t*, whereupon the integral of the peak area is

$$\int \frac{dq_p}{dt} dt = q_p = \Delta H. \tag{4.2}$$

The resulting enthalpy values can be used when calculating the degree of crystallinity of polymers with Equation 2.7 [21, p. 76].

Care must be however taken when interpreting DSC curves. In the compensation DSC, endothermic reactions are usually above the baseline. In other words, they are positive due to higher heat flow directed into the sample than to the reference. In the case of DTA or heat flux DSC, they are directed exactly the opposite way. For this reason it is important to mark the direction of the heat flow. [58, p. 57]

Several factors affecting DSC curves should also be taken into account, including the heating rate, sample mass, calibration, and the purge gas. At high heating rates the reaction occurs slowly, which widens the peaks and shifts them to higher temperatures. This will eventually lead to the decreased resolution. [6, pp. 22–23; 60, pp. 27, 40] The large size of the sample leads to a temperature gradient within it: decomposition of surface and bulk does not occur at the same rate [2, pp. 22–23]. Secondly, it will take more time the sample to melt. This causes discontinuity in the curve, while the thermal gradient appears as a decrease in the slope. Simultaneously peak maximum moves to higher temperatures. [60, pp. 27, 31]

4.3 TMDSC

Temperature modulated DSC (TMDSC) techniques were first introduced by Reading et al. [8]. The great advantage of them, compared to conventional DSC, is their ability to separate the reversing and non-reversing components of the heat flow. In TMDSC a periodic waveform of small amplitude is superimposed on the linear temperature ramp. [7] The most common waveform is a sine wave, which is used in both modulated DSC (MDSC, TA Instruments) [8] and alternating DSC (ADSC, Mettler Toledo) [61]. Other possible temperature fluctuations are the temperature steps followed by isothermal segments, sawtooths (in Steady-State ADSC), and a non-periodic stochastic modulation

[9; 10]. The latter is used in a new multi-frequency TMDSC technique called TOPEM, which will be covered in more detail in the next subsection (4.4).

When the common temperature program is overlaid with a sinusoidal temperature fluctuation, the temperature program can be expressed by the following equation

$$T(t) = T_0 + \beta_0 t + A_\mathrm{T} \cdot \sin(\omega t), \tag{4.3}$$

where T_0 is the initial temperature, β_0 is the underlying heating or cooling rate, A_T is the amplitude of the temperature fluctuation, and ω is the angular frequency of modulation. [62] Two assumptions are made concerning all TMDSC techniques: firstly a sufficiently long time interval and a small temperature modulation are needed in order to consider the DSC as a linear, time-independent system. Secondly the non-reversing reactions can be thought to be so slow that they do not fit in the time scale defined above. On the basis of the first assumption Equation 4.3 can be derived with respect to time, whereupon it can be seen that the resulting heating rate is not constant [8; 63]

$$\frac{dT}{dt} = \beta_0 t + A_T \cdot \omega \cdot \cos(\omega t). \tag{4.4}$$

The curves obtained from a TMDSC measurement are the total heat flow, the non-reversing heat flow, the reversing heat flow, and the complex heat capacity curve. The heat flow into the sample is composed of two components:

$$\phi(T,t) = C_\mathrm{p}\beta + f(T,t). \tag{4.5}$$

The first part of the equation is the reversing heat flow that is related to the heat capacity of the sample, while the second part, *f(T,t)*, is the non-reversing heat flow originating from kinetic processes in the sample. [8; 64] In the case of a sinusoidal modulation the measured heat flow is

$$\phi(T,t) = C_\mathrm{p}(\beta_0 + A_\mathrm{T} \cdot \omega \cdot \cos(\omega t)) + f'(T,t) + C \cdot \sin(\mathrm{wt}), \tag{4.6}$$

where *f'(T,t)* is the underlying kinetic function, when the effect caused by the sine wave modulation has been subtracted, *C* is the amplitude of the kinetic response to the modulation, and ($\beta_0 + A_\mathrm{T}\omega\cos(\omega t)$) is the sinusoidal heating rate. The total heat flow, φ_total, can be calculated from the measured modulated heat flow rate by averaging over at least one modulation period. It is the same as a conventional DSC curve obtained at the same underlying heating rate. [65, pp. 104–105] The non-reversing heat flow in turn is the difference between the total heat flow and the reversing heat flow [13; 64]:

$$\phi_{non} = \phi_{tot} - \phi_{rev}. \tag{4.7}$$

Alongside the ability to separate the reversing and the non-reversing heat flow components, the great advantage of the TMDSC techniques is determination of the glass transition by using the reversing signal, which does not depend on thermal history. High heating rate of the modulation component and the Fourier transform results in a good signal-to-noise ratio, while lowering the scan rate ensures high resolution. However, choosing of the right experimental parameters can sometimes be difficult. The temperature program should be such that the sample is able to follow it, while the region of interest undergoes at least six modulations. For these reasons slow underlying heating rates should be used, which extend the measuring time. There are also transitions, for which TMDSC is not a suitable method and the data obtained by TMDSC should be compared to the conventional DSC measurements. [57, p. 112; 58, p. 62; 63]

4.4 TOPEM

In the basic TMDSC methods temperature-dependent and time-dependent processes can be separated. What makes TOPEM different compared to the former methods is its capability to use different frequencies in a single scan. For TMDSC techniques it was only possible to use a sinusoidal temperature modulation of one frequency at a time. In TOPEM a large number of frequencies is enabled by using a stochastic modulation, which means that overlaying is done by random temperature pulses of different durations. [66] The resulting curve of the TOPEM measurement is the heat flow signal as a function of time. From this the software calculates four curves: total heat flow, reversing heat flow (a sensible heat flow), non-reversing heat flow (a latent heat flow), and quasi-static heat capacity, c_{p0}. The ability to determine the latter is one of the other strengths of TOPEM compared to usual TMDSC techniques. [12]

The assumptions made for other TMDSC techniques are the same in the case of TOPEM. The system includes the DSC instrument and a sample placed in a crucible. The input signal is the measured heating rate, which originates from the constant underlying heating rate and the heating rate of the stochastic temperature modulation. The output signal results from the measured heat flow, which is the sum of the sensible and latent heat flow. The principle of the signal flow is shown in Figure 4.2.

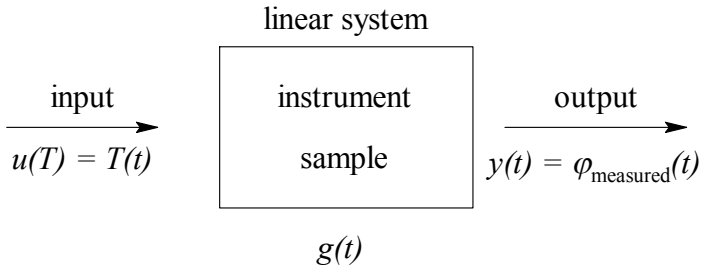

Figure 4.2 *The operating principle of TOPEM. Adapted from [12; 67].*

The input signal, *u(T)* is a superimposition of an underlying temperature program $T_u = T_0+\beta_u t$:

$$u(T) = T(t) = T_u + \delta T(t) = T_0 + \beta_u t + \delta T(t), \tag{4.8}$$

where $\delta T(t)$ is the stochastic temperature modulation, T_0 is the starting temperature, β_u is the constant underlying temperature program or the underlying heating rate, and t is time. [67] The output signal *y(t)* or measured heat flow can be derived from the input signal and the pulse response, *g(t)* of the system as follows

$$y(t) = \varphi_{\text{measured}}(t) = g(t) * u(t) = \int_0^\infty g(\tau)u(t-\tau)d\tau. \tag{4.9}$$

When the non-reversing reactions are assumed to be slow enough, a DSC system is said to be characterized by *g(t)*, which can also be called a transfer function. [12]

4.4.1 Z-transformation

After the non-reversing processes are ignored, the next task is to determine the transfer function in the required time frame. The technique used to solve this is a discrete Laplace transformation in the z-plane called as a z-transformation. With it one can convert a sequence of real or complex numbers, which are discrete time-domain signals, into a complex frequency-domain representation. This simplifies the solving of equations of the time domain. When the convolution property of the z-transformation is applied to Equation 4.9, it can be expressed in the z-plane as follows

$$y(z) = H(z)u(z), \tag{4.10}$$

where terms *y(z), H(z)*, and *u(z)* refer to the z-transforms of *y(t)*, *g(t)*, and *u(z)*. The term *H(z)* can be written by using a rational function

$$H(z) = \frac{B(z)}{A(z)}, \tag{4.11}$$

where *B(z)* and *A(z)* are polynomials of degree q and p, respectively. When this is substituted to Equation 4.10 the following relation is obtained

$$y(z) = \frac{B(z)}{A(z)}u(z) \tag{4.12}$$

and

$$A(z)y(z) = B(z)u(z). \tag{4.13}$$

Applying the inverse z-transformation to Equation 4.13 leads to

$$A(q)y(t) = B(q)u(t), \tag{4.14}$$

where q is the shift operator:

$$q^k y(z) = f(t-k). \tag{4.15}$$

This equation can also be understood as time delay of k time-steps. The polynomials A(z) and B(z) in Equation 4.13 can be written as follows

$$\begin{aligned} a_0 y(z) + a_1 z y(z) + a_2 z^2 y(z) + \cdots + a_\mathrm{p} z^p y(z) \\ = b_0 y(z) + b_1 z u(z) + b_2 z^2 u(z) + \cdots + b_q z^q u(z), \end{aligned} \tag{4.16}$$

which turns, after applying time delay to it, to the following form

$$\begin{aligned} a_0 y(t) + a_1 y(t-1) + a_2 y(t-2) + \cdots + a_\mathrm{p} y(t-p) \\ = b_0 y(t) + b_1 u(t-1) + b_2 u(t-2) + \cdots + b_\mathrm{q} u(t-q). \end{aligned} \tag{4.17}$$

Equation 4.17 simplifies to

$$\sum_{l=0}^{p} a_\mathrm{l} y(t-l) = \sum_{k=0}^{q} b_\mathrm{k}\, u(t-k), \tag{4.18}$$

where a_i and b_i are the unknown parameters of the polynomials *A(z)* and *B(z)*.This equation can be solved by using the prediction-error method (PEM), which is a state-of-the-art mathematical method. In other words the measured input and output quantities are used combined with the least squares fit method in the specific time interval. [12; 68; 69, pp. 16–17, 74]

When there are non-reversing phenomena present in the reaction, Equation 4.18 changes to the following form

$$\sum_{\mathrm{l}=0}^{\mathrm{p}} a_\mathrm{l} y(t-l\Delta t) = \sum_{\mathrm{k}=0}^{\mathrm{q}} b_\mathrm{k}\, u(t-k\Delta t) + \phi_\mathrm{non}(t, c_\mathrm{n}), \tag{4.19}$$

where $\phi_\mathrm{non}(t, c_\mathrm{n})$ is the non-reversing heat flow and c_n is a parameter used to describe this term. [63]

4.4.2 Reversing and non-reversing heat flow

The conventional DSC measurements are performed either under isothermal conditions or the heating and cooling rates are kept constant. The conventional methods are good when the thermal events do not overlap, but when they do, TMDSC methods, like TOPEM, are more effective. With them the separation of the sensible and latent heat flow components or in other words the reversing and the non-reversing heat flow, respectively, is possible. [67]

The reversing and the non-reversing heat flows are calculated from the measured heat flow. The sum of these two curves is the total heat flow:

$$\phi_{\mathrm{total}}(t,T) = \phi_{\mathrm{reversing}}(t,T) + \phi_{\mathrm{non-reversing}}(t,T). \tag{4.20}$$

The reversing heat flow can be written as follows

$$\phi_{\mathrm{rev}}(t,T) = mc_{\mathrm{p0}}(t,T)\beta, \tag{4.21}$$

where m is mass, $c_{\mathrm{p0}}(t,T)$ is the specific heat capacity, and β is the heating rate. The reversing heat flow arises from the heat exchange between the instrument and the sample, which causes the temperature in the sample to change. Because the heat requires long time to be removed, sensible heat can only be measured under quasi-static conditions. [12; 70] The non-reversing heat flow in turn is

$$\phi_{\mathrm{non}}(t,T) = m\Delta h_{\mathrm{i}}\frac{d\alpha}{dt}, \tag{4.22}$$

where Δh_{i} is the specific enthalpy of a thermal event and α is the extent of reaction. It describes the process, which begins far away from equilibrium. [12; 71]

The non-reversing heat flow is the latent heat flow part of the measured heat flow and it derives from a chemical or physical reaction of the sample. That can, for example, be non-reversible chemical reaction, crystallization in supercooled liquids, melting accompanied by supercooled crystallization or vaporization process. These kinds of processes are dependent on the variables that occur far from an equilibrium state, as opposed to reversible reactions that take place close to a local metastable state. [67; 71]

4.4.3 Quasi-static heat capacity

The pulse response is used for calculating the frequency independent quasi-static heat capacity, c_{p0}:

$$m \cdot c_{\mathrm{p0}} = \int_0^\infty g(t)dt. \tag{4.23}$$

It is connected to the heat capacity, which is gained from conventional measurements.

Other parameters that can be calculated from c_{p0}, are in-phase heat capacity, $c'_{p,fi}$, out-of-phase heat capacity, $c''_{p,fi}$, complex heat capacity $c^*_{p,fi}$, and phase. The user can self- select at which frequencies the curves are calculated. The resulting values are used when investigating the glass transition region. They give information about the frequency dependence of T_g. [12]

4.4.4 Temperature program

In ideal case a stochastic temperature modulation of the underlying heating rate is based on step-shaped pulses, which have small height and whose duration or width changes randomly. The temperature fluctuation is given by

$$\delta T(t) = \delta T_0 f_{\mathrm{mod}}(t), \tag{4.24}$$

where δT_0 is the maximum temperature fluctuation and $f_{mod}(t)$ is the modulation function (Figure 4.3), which varies between ±1. The time between separate pulses, the pulse width, is called the switching time range, which is limited by the minimum, Δt_{min}, and the maximum limit, Δt_{max}. These values can be chosen by the user, while the default values are set as 15 s for minimum and 30 s for maximum. [71]

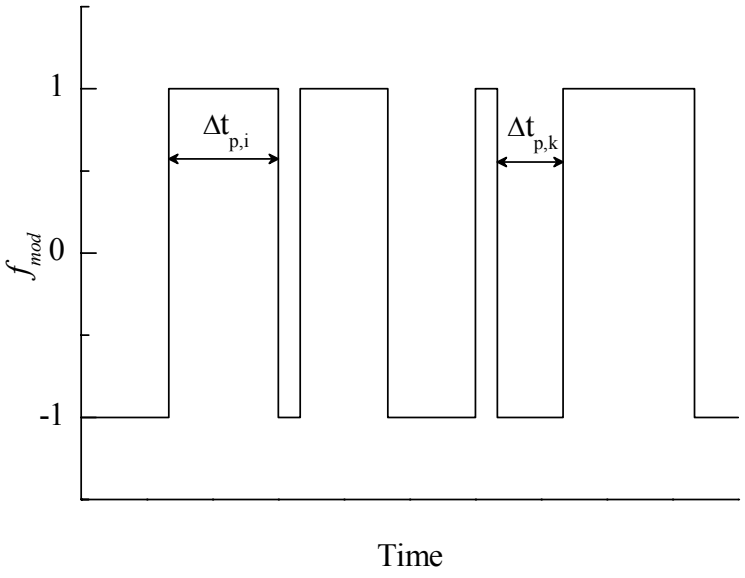

Figure 4.3 *Example of a modulation function, f_{mod}. Terms $\Delta t_{p,i}$ and $\Delta t_{p,k}$ describe different pulse times. Adapted from [71].*

The maximum temperature fluctuation, δT_0, or the amplitude of the temperature pulse, is important value concerning linearity conditions. For glass transition and cold crystallization, suitable value is 0.5 °C, but when there is a critical phase transition, this value should be smaller, namely 0.001 °C. [71]

Figure 4.4 illustrates an example of the temperature program. The straight line is the underlying temperature program, which is overlaid by the modulated pulses. It can be seen that the DSC cell temperature cannot follow the modulation exactly, because it is not able to immediately change the temperature due to the inertia of the system. [72]

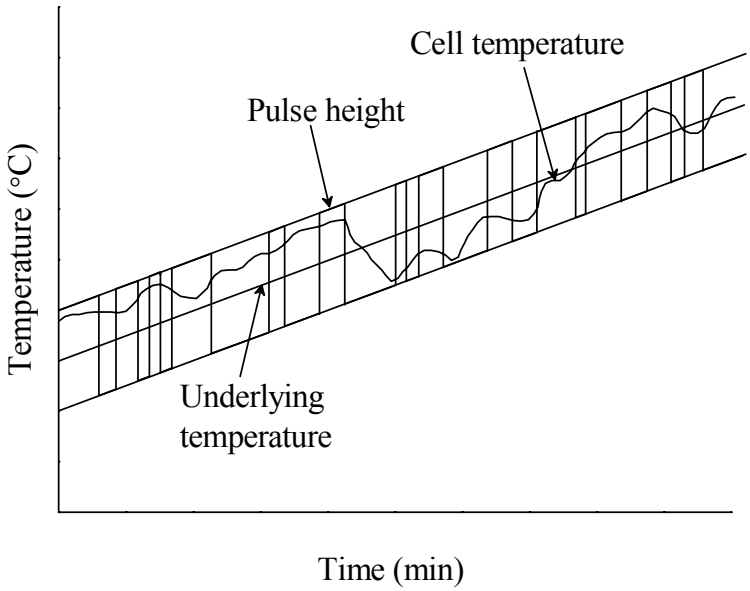

Figure 4.4 *Example of a temperature program used in TOPEM method. Adapted from [12].*

In order to get the curves of the quasi-static heat capacity, the total heat flow, the reversing heat flow, and the non-reversing heat flow, the measured heat flow curve is evaluated by using the method described in the previous chapter. For this, the following calculation parameters have to be determined: the width of the calculation and the smoothing window and the shift of the calculation window (Figure 4.5).

The width of calculation is the time interval within which variation of the non-reversing component is slow enough. It is recommended to be less than one third of the transition interval observed in the heat flow curve. This definition, however, has proven to be too broad by Fraga et al. and they suggested that the width should be less than about one tenth. The default is set at 120 s. The time values smaller than this can result in noise, while too large values cause decreasing of peaks. [66; 72]

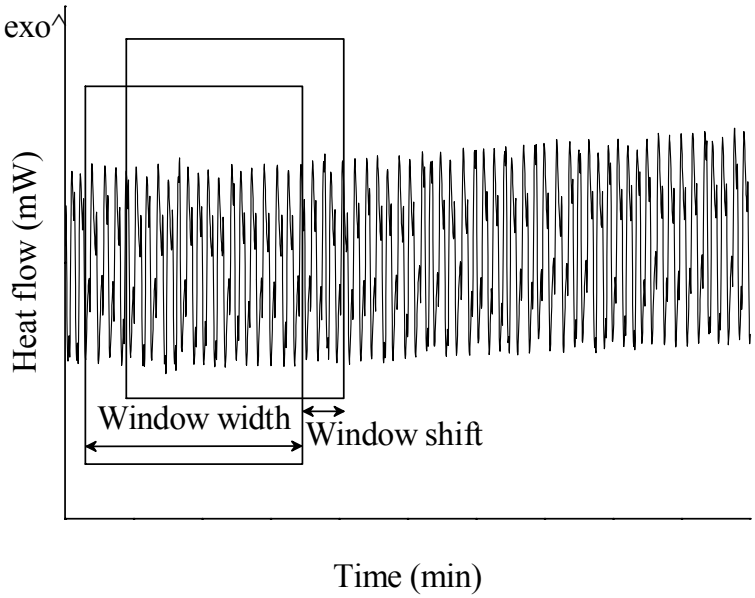

Figure 4.5 *A calculation window of a certain width is shifted along the measured heat flow curve in order to gain the evaluation.*

After every shift of the calculation window by certain time increment a new calculation is carried out. This means that the calculation time is smaller when using higher shifting values, but this may also result in noise. The shift of the calculation window is usually 10 s. The window used for the smoothing filter covers a certain time interval, which is also called the width of the smoothing window. Wider smoothing window prevent noise, but again too large values can smooth non-reversible effects, as well. For this reason, the value of 90 s is recommended. [72]

4.4.5 Advantages and disadvantages of TOPEM

The stochastic modulation used in the TOPEM method enables one measurement over a large frequency range as a function of both time and temperature. This eases the separation of effects that shift with frequency (e.g. glass transition) and those that are frequency-independent (e.g. loss of moisture). The frequency range is broadened by the PEM technique, which also removes the effects originating from the instrument. With TOPEM it is also possible to determine the quasi-static heat capacity and to separate reversing and non-reversing processes. [12]

Although TOPEM is a promising method it has some disadvantages too. It is not a suitable method to measure melting of pure substances (e.g. indium). This is due to inability of the sample to follow a temperature modulation because its temperature does not change during the melting process. Secondly, the linearity of the measurement must be confirmed when studying other melting processes. [13] Choosing the right evaluation parameters can also be difficult. The shape of curves varies significantly with different values and the poorly chosen parameters can result in wrong results. [73]

5 FOURIER TRANSFORM INFRARED SPECTROSCOPY

Infrared (IR) radiation occurs between the visible and microwave regions in the electromagnetic spectrum. It is divided in three regions, namely the near-infrared (14.290–4000 cm^{-1}), the mid-infrared (4000–400 cm^{-1}), and the far-infrared region (700-200 cm^{-1}). An organic molecule can absorb specific frequencies of infrared light, which correspond to the frequency of the particular bond or group vibrating. A technique used to measure this absorption is called Fourier transform infrared (FTIR) spectroscopy. Measurements performed by it are usually carried out in the mid-infrared region. [18, p. 3; 74, p. 369]

IR spectra consist of vibrational bands arising from different types of molecules. Different structures have characteristic wavelengths, λ (μm), at which they absorb light and when band intensity is plotted against wavenumber, $\bar{\nu}$ (cm^{-1}), the characteristic wavelengths can be located in the spectrum. Wavelength, which was used earlier in the literature, can be converted to wavenumber as follows

$$\bar{\nu} = \frac{1}{\lambda}. \tag{5.1}$$

The band intensities can be expressed either in absorbance (A) or transmittance (T). The transmittance is usually used, when analyzing spectra, while absorbance units are for quantitative work. [18, p. 3; 75, pp. 71–72]

5.1 Instrument

Operating principle of the transmission technique is illustrated in Figure 5.1. The source sends a light beam with an intensity of I_0, which travels through the sample to the detector. The sample absorbs some wavelengths of light, which results in the altered intensity, I. The absorbance spectrum can be calculated then from the ratio of I_0 and I with the following equation

$$A = \log(I_0/I), \tag{5.2}$$

where A is the absorbance. The absorbance in turn is related to the concentration of the molecules in the sample. This connection is also known as the Lambert-Beer's law:

$$A = \varepsilon cd, \tag{5.3}$$

where ε is the molar absorption coefficient, c is concentration, and d is the thickness of the sample. [18, pp. 5–6] For this reason absorbance units should be used for quantitive analysis [18, p. 149].

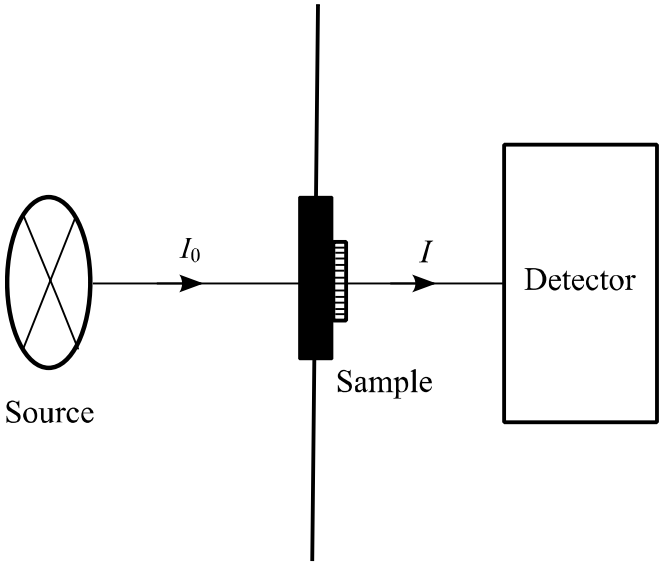

Figure 5.1 *Schematic view of an instrument operating with the transmission technique. Adapted from [74].*

When spectra are expressed in transmittance units, Equation 5.2 transforms to the following form

$$\%T = 100 * \log(I_0/I), \tag{5.4}$$

where $\%T$ is percent transmittance. Because transmittance is mathematically related to absorbance, $\%T$ units can be easily converted into the absorbance units and vice versa. [18, pp. 5–6] Typical samples analyzed with the transmittance mode are thin films, liquids, and solids. KBr technique is usually used for powders and solid materials. In this method KBr and sample powders are mixed together and the mixture is exposed to pressure. Only sample particles are visible in the resulting pellet, for KBr is transparent in the measurement region. KBr tablets are also used when measuring liquid samples. The drop of liquid is placed between two pellets, which are positioned in a sample holder. Thin films are prepared by a cast film technique, in which the sample is dissolved in a suitable solvent. The solution can be casted over KBr tablet or flat surface, from where the resulting film is then removed. [72, pp. 87, 89–90, 100, 106]

Another experimental technique is attenuated total reflectance (ATR), which is meant especially for samples that are too thick or whose absorbance is too high to be

determined by transmission technique. It can also be used in cases when the sample should stay undamaged. The principle of the ATR technique is shown in Figure 5.2.

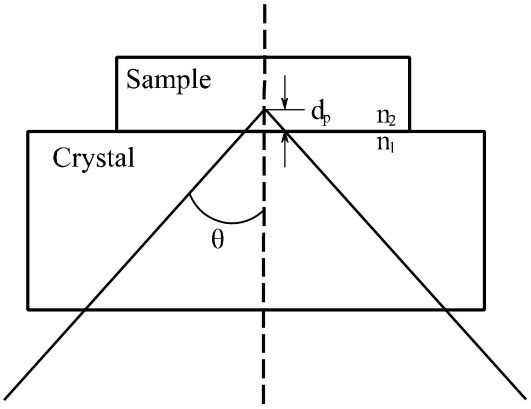

Figure 5.2 *Operating principle of the ATR technique. A Sample is positioned on a crystal through which light is directed to the sample at an angle of θ. The crystal has a greater refractive index (n_1) than the sample (n_2). Light penetrates a few wavelengths (d_p) into the sample. Adapted from [18].*

The sample is positioned on a crystal through which the light beam is directed to the sample at a certain angle. Because the refractive index of the crystal (n_1) is higher than the one of the sample (n_2), light penetrates a few wavelengths (d_p) into the sample and reflects then back. [74, p. 371]

5.2 Advantages and disadvantages of FTIR

FTIR is a relatively easy method to study the properties of polymers. The measurements are fast and preparation of a sample can be carried out easily without damaging it. IR light does not change the sample, thus it can be measured repeatedly. In addition, FTIR has high signal-to-noise ratio and is a very sensitive technique. [18, p. 14; 74, p. 376]

However, the presence of water or carbon dioxide can complicate interpretation of spectra, while their absorption bands can overlap with the other bands. Impurities present in the sample cause also appearance of additional peaks. The one drawback of transmission technique is the opacity problem, which means that a too concentrated sample absorbs all the light resulting in broad and misshaped peaks. [18, pp. 16, 87–88; 74, p. 376]

6 EXPERIMENTAL

The materials and methods used in this study are described in this chapter. Semicrystalline P(L/D)LA with various compositions was investigated by DSC. Thermal analysis of multiple melting behavior of PLA was performed by using the new temperature-modulated technique termed TOPEM and the results were compared to the ones obtained with conventional DSC. Also, the plasticizing effect of water on amorphous PDLLA was investigated by FTIR. All the measurements were done with a transmission technique and the transmittance units were converted into the absorbance units in order to obtain the quantitative results.

6.1 Materials

Poly(L/D-lactic acid) with a 1 and 4% of D-lactic acid content (P(L/D)LA 99/1 and 96/4) was purchased in the form of granules, from which the samples of suitable mass and shape were cut for DSC measurements. The material was used directly without further purification or treatment.

Samples for FTIR analysis were prepared from medical grade poly(D,L-lactic acid) (PDLLA, R207 S) powder which was obtained from Böhringer Ingelheim. The weight average molecular weight and the number average molecular weight of the raw material were 225,287 and 100,847 g mol^{-1}, respectively. The polydispersity index of the untreated polymer was 2.23. After gamma sterilization molecular weights were 68,842 and 34,526 g mol^{-1}, while the polydispersity index was 2.19.

PDLLA powder was dissolved in acetone and the solution was casted on a Petri dish. The resulting film was carefully removed and stretched over round mountings, to where they were attached by a PLA string in a manner indicated in Figure 6.1.

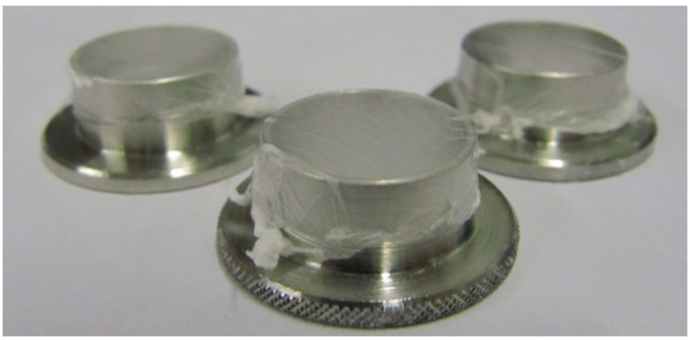

Figure 6.1 *The PDLLA cast films attached to the mounting frames by the PLA string.*

Three of the films were gamma sterilized before the measurements, while the other three were left untreated. All cast films were dried in vacuum before the analysis in order to remove remaining water.

6.2 Differential scanning calorimetry

Measurements of thermal behavior of PLA were performed with a Mettler Toledo DSC1 differential scanning calorimeter equipped with sample robot and liquid nitrogen cooling accessory. STAR^e software was used to control the experiments and to evaluate the measured curves. The instrument was calibrated by using indium, zinc, water, and heptane as standards. Polymer samples of *ca.* 6 mg were weighed and sealed in aluminum pans with pierced lids. Scans were carried out under a nitrogen flow of 60 ml min^{-1}.

6.2.1 Dynamic DSC analysis

The dynamic DSC scans without crystallization were carried out from 5 to 200 °C at the heating rate of 20 °C min^{-1}. This method was also used to remove the thermal history of the samples before each measurement. All DSC curves were normalized with respect to the sample mass and reference temperature.

6.2.2 Isothermal DSC analysis

Multiple melting behavior of PLA was studied by crystallizing the samples isothermally at various temperatures. First, thermal history of the samples was erased by heating them from room temperature to 200 °C at the heating rate of 20 °C min^{-1}, after which they were first cooled to 0 °C and then heated to the desired crystallization temperature (T_c) at the rate of 5 °C min^{-1}, where they were held for one hour to attain crystallized structure. This treatment was followed by cooling the samples back to 0 °C. Finally the samples were reheated from 0 to 200 °C at the rate of 5 °C min^{-1} in order to study the melting behavior.

The crystallization of the samples was also performed for three hours. The temperature programs used were almost similar than described above but the heating and cooling rates were faster, namely 20 °C min^{-1} in each section.

6.2.3 TOPEM analysis

Suitable measurement parameters for TOPEM analysis were determined by preliminary studies. The heating rates of 0.1–0.5 °C min^{-1} and the pulse heights of 0.005–0.05 °C were tested. A suitable width for the calculation window was determined by comparing the total heat flow curve to the mean value of the measured heat flow curve.

After preliminary measurements the following parameters were chosen: TOPEM analyses of P(L/D)LA 99/1 were performed by using the underlying heating rate of 0.25 °C min^{-1} and the pulse height of 0.05 °C. Evaluations of the measured heat flow curves

were done by using the calculation window of 225 s. In the case of P(L/D)LA 96/4 the underlying heating rate was 0.5 °C min^{-1} and the pulse height was 0.05 °C. The width of the calculation window used was 175 s. Default values of other parameters were used: the switching time range was set as 15–30 s, the shift of calculation window was 10 s and the width of smoothing window was 90 s.

The samples were analyzed both without any pretreatment and after crystallization for one and three hours at various temperatures. The methods used for crystallization were the same as in the conventional DSC measurements, except for the last heating segment, which was replaced by the TOPEM scan.

6.3 FTIR Spectroscopy

FTIR spectra were measured with a Perkin Elmer Spectrum One FT-IR Spectrometer at a resolution of 4 cm^{-1}. For every spectrum 8 scans were done from 4000 to 450 cm^{-1} in a transmission mode and the resulting spectra were converted to absorbance format.

After the first measurement the samples were placed into a drying oven at the temperature of 37 °C. Two of the films (Film 1 and Film 2) were put into water, which was tempered beforehand to 37 °C, while the third film (Film 3) was kept in the oven without water treatment. Film 1 was measured with FTIR after 24 hours and again after 48 hours. Film 2 was kept in water without intermediate measurements and was analyzed next time after one week of immersion. Third film (Film 3), which was kept in the oven without water treatment, was measured at the same times as Film 1.

Films 4-6 were gamma sterilized. Similar procedure was carried out to them as in the case of first three films: Film 4 underwent water treatment with intermediate measurements, while Film 5 was kept constantly in water for seven days. Film 6 in turn was kept in the oven without water treatment.

In order to compare the results for both untreated and gamma sterilized samples the curves were normalized. This was done by using the signal of the band, which is shared by all the samples and stays unchanged during water treatment. The spectrum of the vacuum dried Film 1 was used as reference for all of the spectra, which were normalized with respect to absorption intensity of the asymmetric bending of the CH_3 group at 1454 cm^{-1}. The band is stated to be a suitable standard due to its isolated position in the spectrum. Additionally its wavenumber does not change during water treatment and there are only slight changes in intensity. Normalization should remove the experimental error arousing from the different thicknesses of the samples. [76] Because the baseline deviated from zero absorbance, the real absorbance of the peak was obtained by subtracting the bottom value from the peak maximum.

7 RESULTS AND DISCUSSION

The results obtained for poly(lactic acid) of different compositions are presented below. Multiple melting behavior of PLA has already been widely investigated by the conventional DSC method, which provides a large number of materials for comparing the results obtained with the conventional DSC in this work. As for TOPEM measurements, they are compared to analogous studies performed by basic TMDSC methods. Additionally, the results obtained from FTIR analysis are given and compared to the reference values. The possible explanations for observed events are discussed in each case.

7.1 Conventional DSC measurements of P(L/D)LA 99/1 and 96/4

The peak temperatures and crystallinity values of P(L/D)LA 99/1 and 96/4 measured by the conventional DSC method are presented in Table 7.1. The heating scan from 5 to 200 ºC with the heating rate of 20 °C min^{-1} was performed twice to examine the behavior of the samples before and after removing the thermal history. The degree of crystallinity was calculated from Equation 3.1 by using a value of 93.1 J g^{-1} for the heat of fusion of the pure PLLA crystal [45]. In Figure 7.1 the DSC curves of both samples obtained during the first and second heating scans are illustrated.

Table 7.1 *Thermal characteristics of the PLA samples with different D-content.*

Material	Scan	T_g (ºC)	T_c (ºC)	T_m (ºC)	X (%)
P(L/D)LA 99/1	1st	68.43	157.87	171.51	39.4
	2nd	60.01	128.87	167.41	1.3
P(L/D)LA 96/4	1st	65.08	-	156.65	37.5
	2nd	62.49	116.23	149.53	0.1

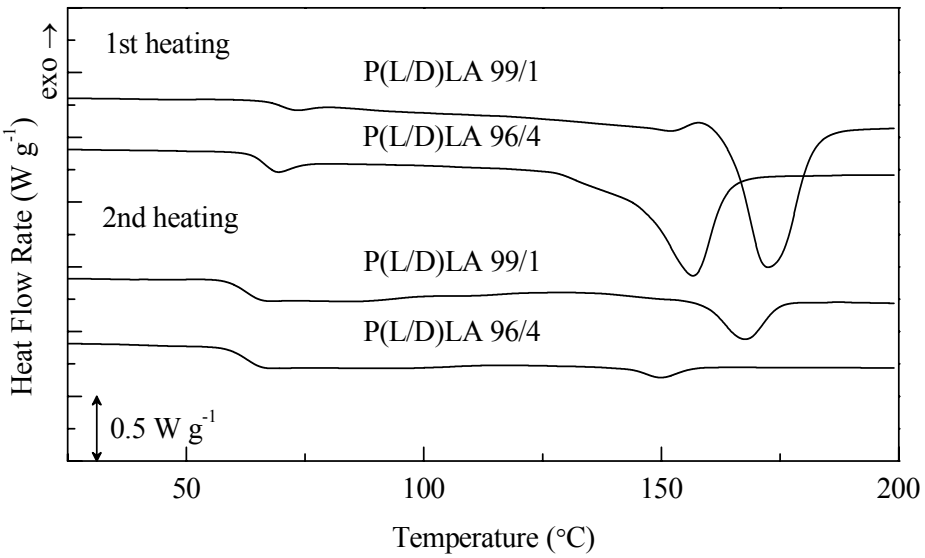

Figure 7.1 *DSC curves of P(L/D)LA 99/1 and 96/4 for the first and second heating scans. The curves have been shifted vertically for clarity.*

The first heating curve of P(L/D)LA 99/1 is characterized by the glass transition at 60.01 ºC and the melting peak at 171.51 ºC. Prior to the endotherm there is a small exotherm at 157.87 ºC. From the first heating curve of P(L/D)LA 96/4 the glass transition can be detected at 62.49 ºC and the melting peak at 156.65 ºC. The crystallinity value of both samples is *ca.* 40%, which indicates that they are semicrystalline materials. During the second heating scan the areas of endotherms of both samples decrease significantly and the peaks shift to lower temperatures. The small exotherm of P(L/D)LA 99/1 is replaced by a broader one and some crystallization is observed for P(L/D)LA 96/4, as well. The enthalpy relaxation detected in the first heating scan curves is removed and T_g measured during the second scan is higher for P(L/D)LA 99/1 than for P(L/D)LA 96/4.

7.1.1 Crystallization of P(L/D)LA 99/1 and 96/4 for one hour

Isothermal crystallization of PLA was performed at various temperatures (T_c) ranging from 80 to 130 °C. The thermal characteristics of P(L/D)LA 99/1 after one hour of crystallization are shown in Table 7.2. A small exotherm (P_{exo}) at temperature T_{exo} appears at every T_c prior to the single melting peak (P_1) at temperature T_{m1}. At 80 °C, there is also another crystallization peak (P_{cc}) at T_{cc} before P_{exo} due to cold-crystallization. At $T_c \geq 100$ °C, an additional melting peak (P_2) at temperature T_{m2} is observed. The crystallization temperature affects the position of the peaks. The peak values in Table 7.2 show continuous but not linear increase with increasing T_c. In the case of P_1, the change is not as significant compared to the other peak temperatures. The degree of crystallinity varies between 45 and 52%.

Table 7.2 *Thermal properties of P(L/D)LA 99/1 determined after crystallization for one hour at various temperatures.*

T_c (°C)	T_g (°C)	T_{cc} (°C)	T_{m2} (°C)	T_{exo} (°C)	T_{m1} (°C)	X (%)
80	62.69	95.81	-	149.82	167.68	45.3
90	66.18	-	-	151.32	167.83	44.7
100	64.19	-	148.30	155.15	168.24	46.1
110	64.77	-	149.88	154.80	168.59	48.1
118	64.98	-	151.12	155.79	166.53	52.2
120	64.52	-	149.63	-	168.71	50.2
125	64.54	-	151.54	-	168.59	51.2
130	64.42	-	152.54	-	168.59	51.1

Similarly, thermal behavior of P(L/D)LA 96/4 was investigated after one hour of crystallization. Values obtained in the measurements are presented in Table 7.3. At T_c > 90 °C, P_2 appears. The area and the temperature of the peak increase with increasing T_c. Simultaneously, P_1 shifts to the higher temperatures, while its area decreases. Finally, at $T_c \geq 110$ °C, only a single peak (P_1) is observed. The corresponding DSC curves are presented in Figure 7.2 (a) and (b).

Table 7.3 *Thermal characteristics of P(D/L)LA 96/4 recorded after crystallization for one hour at various temperatures.*

T_c (°C)	T_g (°C)	T_{cc} (°C)	T_{m2} (°C)	T_{m1} (°C)	X (%)
80	58.69	124.32	-	151.85	1.4
90	59.33	114.39	142.87	153.31	16.5
100	60.68	-	147.13	154.40	36.1
105	60.36	-	148.52	154.59	39.0
110	60.56	-	-	150.09	35.1
118	60.06	-	-	152.10	39.0
120	59.02	-	-	152.83	39.4
125	59.27	-	-	154.14	40.9
130	59.58	-	-	155.24	40.9

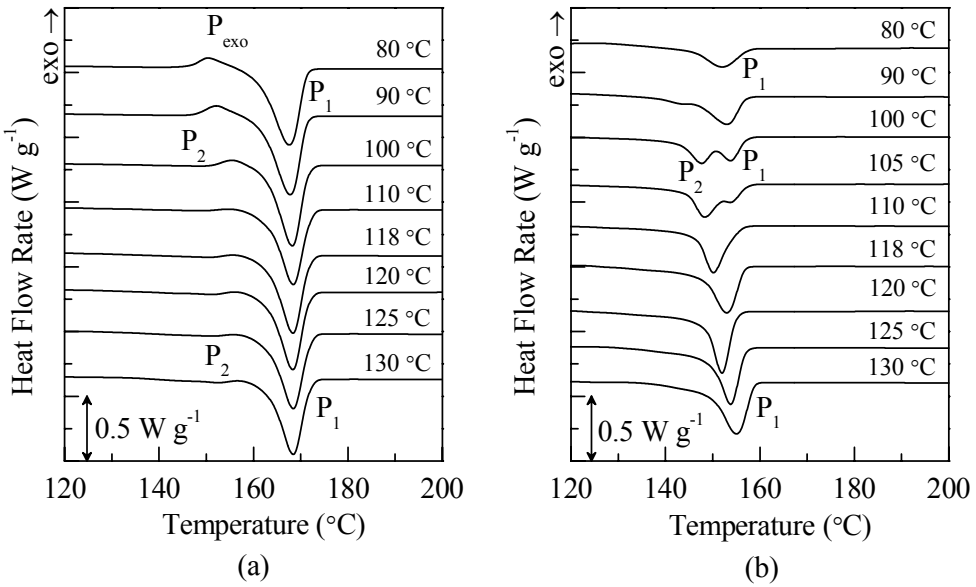

Figure 7.2 *DSC curves obtained for (a) P(L/D)LA 99/1 and (b) P(L/D)LA 96/4 after one hour of crystallization at temperatures between 80 and 130 °C. The curves have been shifted vertically for clarity.*

Clearly, in the case of P(L/D)LA 99/1, one hour is not sufficient for the appearance of the second melting peak. This can be assumed to be due to the higher L-content of the sample compared to P(L/D)LA 96/4, because both endotherms are observed for the latter. Pan et al. attained similar results when studying the effect of molecular weight on the double melting behavior of poly(lactic acid). They observed P_{exo} at $T_c < 100$ °C for the sample with high molecular weight (M_n=118.3 kg mol^{-1}), while in the case of the sample with the lower molecular weight (M_n=15.4 kg mol^{-1}) P_2 is visible instead of P_{exo}. However, they did not report the amounts of the L- and D-enantiomers and referred to the polymer only as PLLA. [15] Based on this, it is difficult to say, whether they had the sample consisting only of an L-enantiomer or whether there was some D-enantiomer in the polymer, as well.

7.1.2 Crystallization of P(L/D)LA 99/1 and 96/4 for three hours

Since one hour was apparently not enough for P(L/D)LA 99/1, crystallization for three hours was carried out. The results presented in Table 7.4 show that in this time P_2 can be observed to appear and disapper in the DSC curves. As in the case of P(L/D)LA 96/4, the peak temperatures of both P_1 and P_2 increase with increasing T_c. At $80 \leq T_c \leq 100$ °C, P_{exo} is observed, while at temperatures above 110 °C it is replaced by P_2. When T_c is above 125 °C, only a single melting peak, P_1, is present. The degrees of crystallinity are relatively high at higher crystallization temperatures.

Table 7.4 *Thermal values of P(D/L)LA 99/1 obtained after crystallization for three hours at various temperatures.*

T_c (°C)	T_g (°C)	T_{cc} (°C)	T_{exo} (°C)	T_{m2} (°C)	T_{m1} (°C)	X (%)
80	60.15	111.32	149.47	-	167.89	28.9
90	65.07	-	151.23	-	168.01	44.1
100	65.01	-	155.63	153.03	168.57	47.8
110	64.49	-	-	162.68	170.02	52.1
115	64.89	-	-	164.35	170.31	52.4
118	62.55	-	-	164.99	170.18	57.5
120	62.06	-	-	165.66	170.21	59.3
125	64.93	-	-	-	166.76	59.8
130	64.43	-	-	-	167.91	61.6

The P(L/D)LA 96/4 sample was also crystallized for three hours in order to determine, whether crystallization time has some influence on the curves. The peak temperatures of thermal events (Table 7.5) show that in this case the endotherms occur at slightly higher temperatures, but apart from that there is no significant difference between them and the ones recorded after one hour of crystallization. Figure 7.3 (a) and (b) show the corresponding DSC curves of both P(L/D)LA 99/1 and 96/4 samples.

Table 7.5 *Thermal characteristics of P(D/L)LA 96/4 measured after crystallization for three hours at various temperatures.*

T_c (°C)	T_g (°C)	T_{m2} (°C)	T_{m1} (°C)	X (%)
80	60.58	-	152.63	7.4
90	61.92	143.53	153.47	32.8
100	61.02	147.56	154.00	37.7
105	61.45	149.03	154.19	37.3
110	60.43	-	150.49	41.2
115	60.07	-	151.81	41.6
118	60.58	-	152.63	41.9
120	60.01	-	153.22	42.6
125	59.73	-	154.66	40.7
130	59.16	-	155.84	41.0

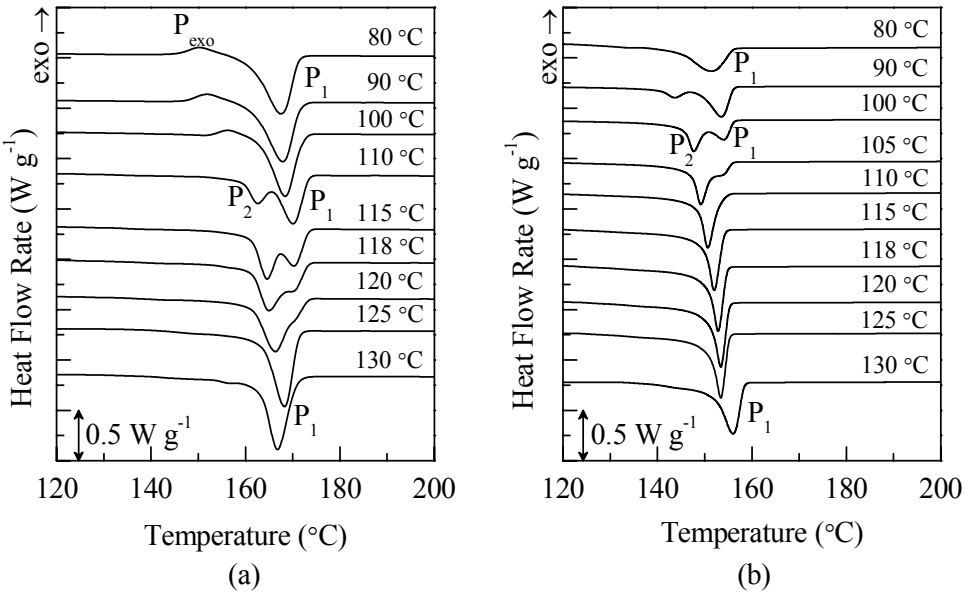

Figure 7.3 *DSC curves of P(L/D)LA 99/1 and 96/4 obtained after three hours of crystallization at temperatures between 80 and 130 °C. The curves have been shifted vertically for clarity.*

From these results it can be concluded that the higher D-content advances the appearance of the second melting peak. In the case of P(L/D)LA 96/4 the temperature range where both endotherms are visible is observed at 20 °C lower temperatures than for P(L/D)LA 99/1.

7.2 TOPEM measurements of P(L/D)LA 99/1 and 96/4

In order to carry out TOPEM measurements, suitable parameters were determined first. While the preliminary studies were performed, it turned out that the samples with different D-content required slightly different experimental conditions. The parameters tested were the underlying heating rate, pulse height, and the width of the calculation window. The latter was also used to ensure the stationarity of the chosen program. The linearity of the measurement was checked by comparing the reversing heat flow curves recorded with two different pulse heights. The chosen parameters were used in TOPEM measurements to study double melting behavior of PLA after one and three hours of crystallization.

7.2.1 Selection of the optimal measurement parameters

The heating rates between 0.1 and 1 °C min^{-1} were tested. The recommended rates are between 0.5 and 2 °C min^{-1}, except in the case of melting, for which the heating rate of lower than 0.1 °C min^{-1} is recommended. The heating rate is known to affect the evaluation parameters, especially the width of the calculation window. That is why care must be taken to select suitable parameters. Influence of the heating rate on the DSC curves

of P(L/D)LA 99/1 and P(L/D)LA 96/4 is shown in Figure 7.4 and Figure 7.5, respectively. The pulse height was set at 0.05 °C in each measurement.

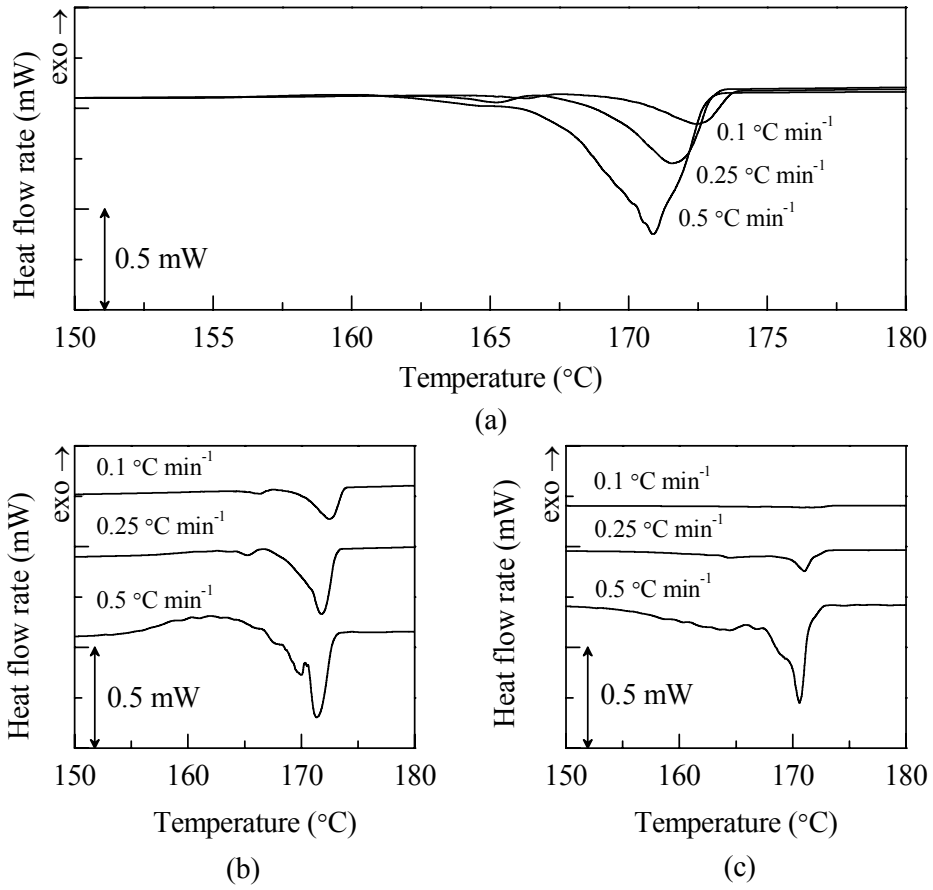

Figure 7.4 *The effect of the heating rate on (a) the total, (b) non-reversing, and (c) reversing heat flow curves of P(L/D)LA 99/1. The pulse height was 0.05 °C and width of calculation window was 225 s. The curves have been shifted vertically for clarity.*

Changing of the heating rate affects all the curves. The peak detected on the total heat flow curve of P(L/D)LA 99/1 shifts to lower temperature and its area increases with an increasing heating rate. However, in the case of the non-reversing heat flow curve, the shape of the peak alters as well. Two lower heating rates, 0.1 and 0.25 °C min^{-1}, are very similar, although the peaks detected with 0.1 °C min^{-1} are quite small. Noise is present in the curves, which were recorded at the heating rate of 0.5 °C min^{-1}. In the reversing heat flow curve there is also a wide exotherm prior to a splitted melting peak. For these reasons the heating rate parameter of 0.25 °C min^{-1} was selected for the following investigations of P(L/D)LA 99/1.

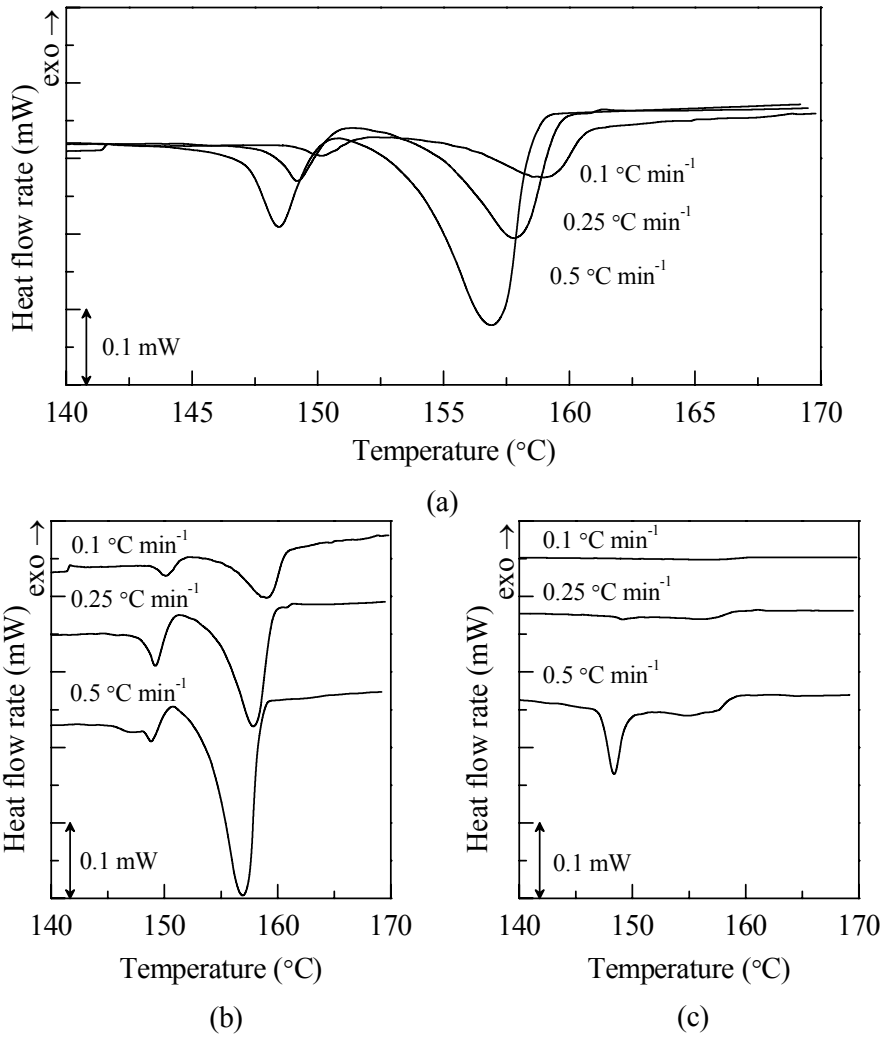

Figure 7.5 *The effect of the heating rate on (a) the total, (b) non-reversing, and (c) reversing heat flow curves of P(L/D)LA 96/4. The pulse height was 0.05 °C and width of the calculation window was 175 s. The curves have been shifted vertically for clarity.*

The effect of the heating rate on the TOPEM curves of P(L/D)LA 96/4 is not as remarkable as for P(L/D)LA 99/1. On the non-reversing and reversing heat flow curves, however, the peaks become relative small and thermal events are harder to distinguish at the slower heating rates. Thus, in this case the heating rate parameter of 0.5 °C min^{-1} was selected for the following measurements of P(L/D)LA 96/4.

The pulse height has also an influence on the melting peak. Recommendation for glass transition, crystallization, and evaporation is ±0.5 °C, which has been set as a default in the software. For melting and phase transitions of first or second order this value should be much smaller, namely between ±0.05 and ±0.001 °C. If the pulse height is set too low, it gives noisy results, whereas too large values induce non-linear conditions. The effect of the pulse height on total heat flow curves is demonstrated in Figure 7.6.

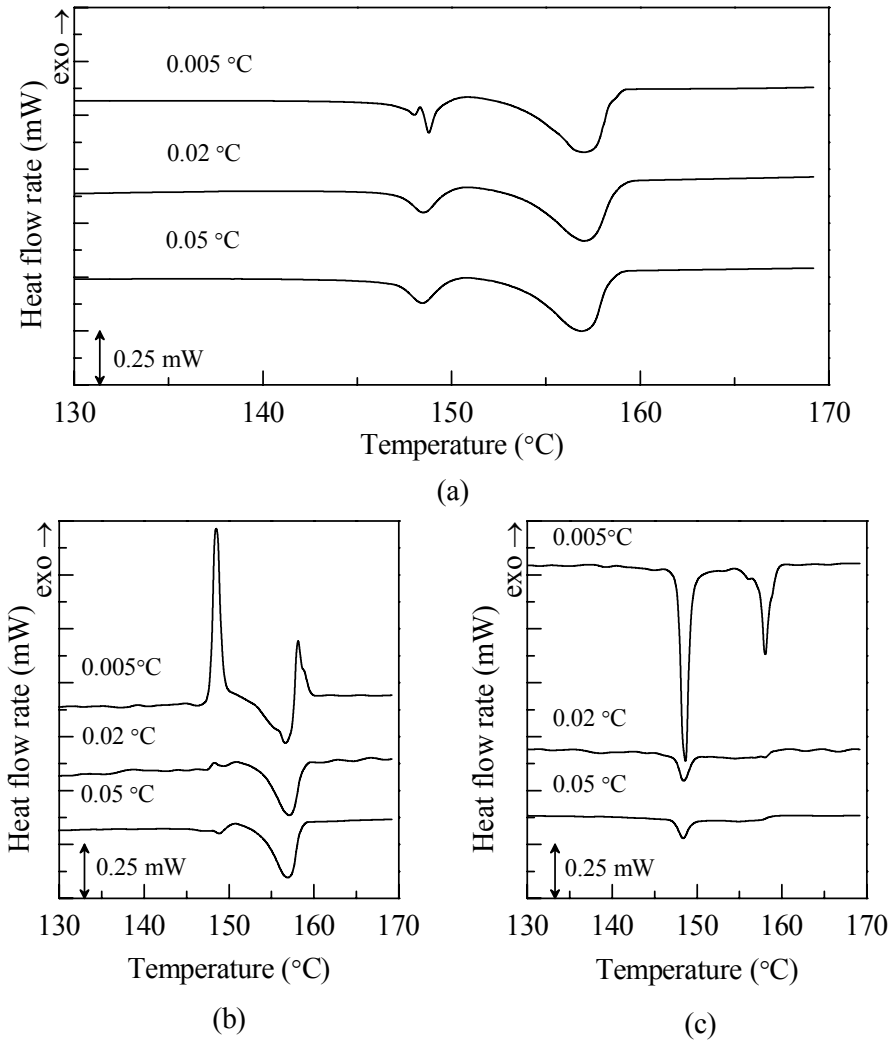

Figure 7.6 *The effect of the pulse height on (a) the total, (b) non-reversing, and (c) reversing heat flow curves of P(L/D)LA 96/4. The heating rate was 0.5 °C min^{-1} and the width of the calculation window was 175 s for each evaluation. The curves have been shifted vertically for clarity.*

Pulse heights of 0.005 °C, 0.02 °C, and 0.05 °C were tested for P(L/D)LA 96/4, while the heating rate was kept as 0.5 °C min^{-1} in each measurement. All of the selected pulse heights are within the limits given for melting. The smallest pulse height can be eliminated easily, because the total heat flow curve differs significantly from the measured heat flow curve. This can also be observed in the non-reversing heat flow curve, where two additional exotherms are present. The total heat flow curves recorded with the pulse heights of 0.02 and 0.05 °C are very similar. However, there is some noise present in the non-reversing and reversing heat flow curves of smaller pulse height. For these reasons the best choice is the pulse height of 0.05 °C. Because this was detected to be a suitable value also for P(L/D)LA 99/1, no further examination was performed in that case.

7.2.2 Stationarity and linearity of the TOPEM measurements of P(L/D)LA 99/1 and 96/4

The response function of the system is calculated from the measured heat flow. For this the user sets a calculation window width, within which the TOPEM evaluation is made. The recommended width is less than or equal to one third of the width of the transition interval. A default value is set as 120 s in the software. [66]

Because the width of calculation window has a great effect on the curves, comparison between different window sizes were made. The correct width should be the one that generates the total heat flow curve having a good fit with the measured heat flow curve, whereupon the stationary condition of the measurement is fulfilled. This was verified by using the method described by Parmentier [73]. The total heat flow curve was subtracted from the measured heat flow curve, after which the amplitudes of the resulting curve were summed up. If there were large variations between the curves, the sum was higher.

The calculation windows obtained from summing of the amplitudes, t_{cw2}, for the PLA samples with different D-content and crystallization times, t_c, are presented in Table 7.6 The width of the calculation window was predicted for each measurement individually, but only one T_c is presented here as an example. At this particular temperature the double melting peaks are visible for both samples. Recommended calculation window, t_{cw1}, was calculated from the transition interval, Δt, by dividing it by three.

Table 7.6 *The transition intervals, Δt, of P(L/D)LA 99/1 and 96/4 obtained with different crystallization times, t_c, temperatures, T_c, and heating rates, β. Calculated widths of the calculation window, t_{cw2}, are compared to the recommended widths, t_{cw1}.*

Sample	t_c (min)	T_c (°C)	β (°C/min)	Δt (s)	t_{cw1} (s)	t_{cw2} (s)	$t_{cw2}/\Delta t$
P(L/D)LA 99/1	60	100	0.25	3120	1040	225	1/14
P(L/D)LA 99/1	180	100	0.25	2880	960	225	1/13
P(L/D)LA 96/4	60	100	0.5	1920	640	175	1/11
P(L/D)LA 96/4	180	100	0.5	1680	560	175	1/10

In the case of P(L/D)LA 99/1 transition intervals and calculation windows are wider compared to P(L/D)LA 96/4. When t_{cw2} is divided by Δt, the obtained ratio is ca. one tenth for both samples. This supports a remark made by Fraga et al. that the recommended width is too broad [66]. Sum of amplitudes is plotted against the corresponding calculation window in Figure 7.7. For P(L/D)LA 99/1 sums are higher because the slower heating rate used results in the higher amount of counting points.

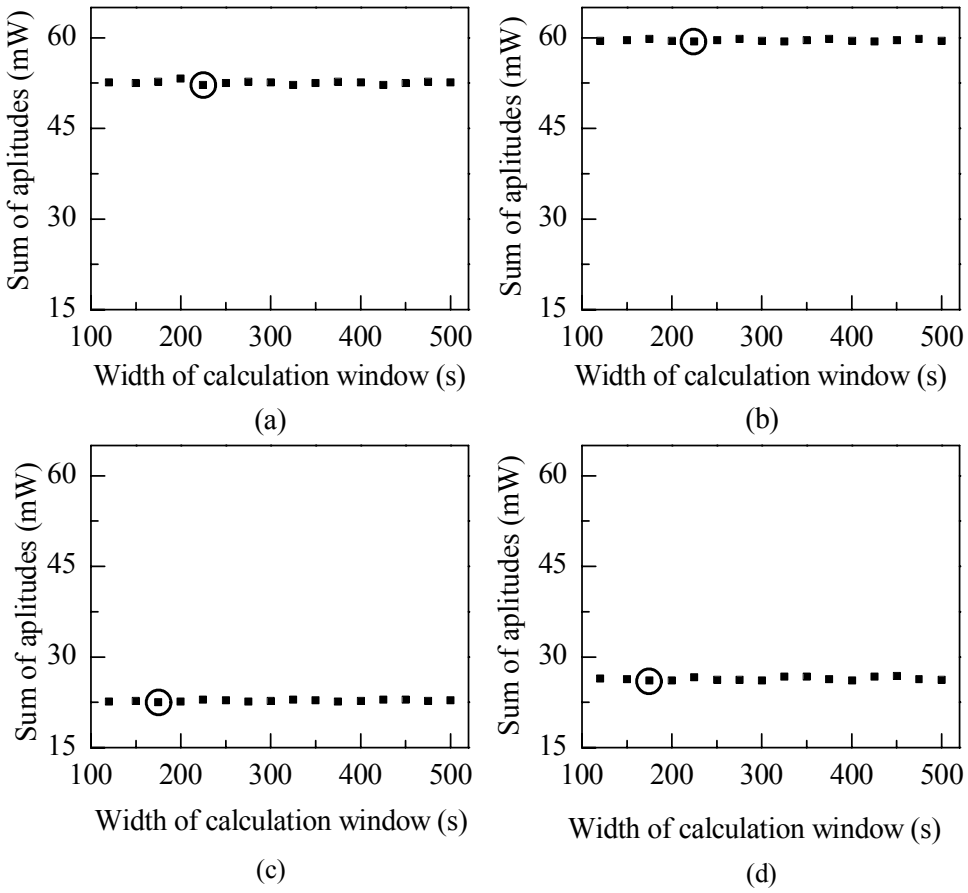

Figure 7.7 *Sum of amplitudes plotted against the different widths of calculation window for P(L/D)LA 99/1 after crystallizing for (a) one and (b) three hours. Similarly, for P(L/D)LA 96/4 after crystallizing for (c) one and (d) three hours. The calculation window with the lowest sum of amplitudes is marked with a circle.*

The difference between the sums is significantly small and the calculation windows with the width close to t_{cw2} give very similar curves. However, the further t_{cw} gets from t_{cw2} the more the total heat flow curve differs from the mean value of measured heat flow. This variation is illustrated in Figure 7.8, where the total heat flow curves of P(L/D)LA 96/4 obtained with t_{cw} ranging between 30 and 800 s are compared to the measured heat flow curve.

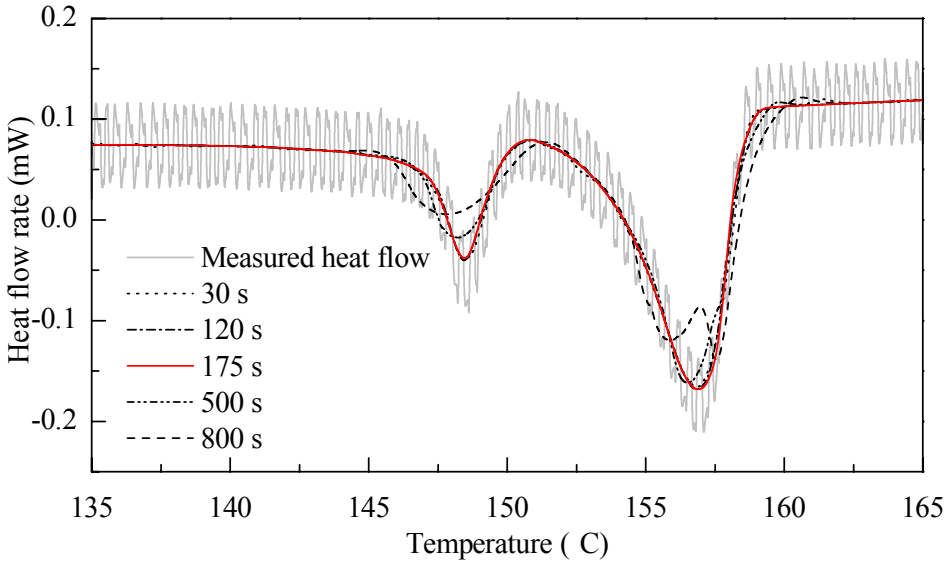

Figure 7.8 *Comparison of the measured heat flow curve (grey) of P(L/D)LA 96/4 and total heat flow curves calculated from it by using the calculation windows with different widths. The sample was crystallized for one hour at 100 °C before the TOPEM measurement. The following TOPEM parameters were used: the underlying heating rate of 0.5 °C min^{-1} and the pulse height of 0.05 °C. The red (solid) curve shows the evaluation done with the calculation window width of 175 s.*

The total heat flow curve follows the average of the measured heat flow curve quite well up to 300 s, but when the width gets over 500 s, curves do not correlate any more. Using the calculation window width of 800 s produces splitted peaks. Even though the total heat flow curves evaluated with t_{cw} close to the best calculated one (175 s) do not differ much, it should be taken into account that the effect can be much greater on the reversing and non-reversing heat flow curves. For this reason they should be examined closely as well when choosing the suitable width. This can however be difficult when the behavior of the sample material is not known beforehand.

The linearity of the measurement should be taken into account as well. This was done by comparing the reversing heat flow curves of P(L/D)LA 96/4 obtained by two different pulse heights (Figure 7.9), while the heating rate used was the same, namely 0.5 °C min^{-1}. The pulse heights of 0.005 and 0.05 °C were used.

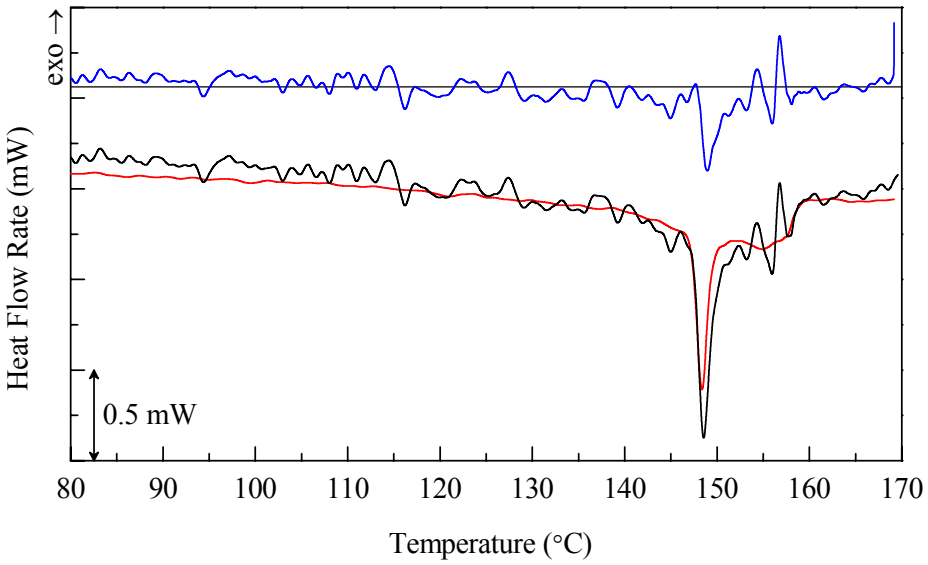

Figure 7.9 *Linearity test performed with TOPEM to P(L/D)LA 96/4, which was crystallized before the TOPEM measurement at 100 °C. Black and red curves are the reversing heat flow curves obtained with the pulse heights of 0.005 and 0.05 K, respectively. The blue curve is the difference between them. The heating rate was 0.5 K/min and the width of the calculation window 175 s.*

Linearity condition is said to be fulfilled if the reversing heat flow does not depend on the intensity of the temperature modulation [13]. The blue curve is the difference between the reversing heat flow curves obtained with different pulse heights. It follows the straight line quite well, and thus it can be concluded that linear conditions are satisfied. However, as stated above, the pulse height of 0.005 °C is not suitable for these measurements.

7.2.3 TOPEM analysis of P(L/D)LA 99/1

The TOPEM measurement performed for P(L/D)LA 99/1 without preliminary crystallization is shown in Figure 7.10. The total heat flow curve is characterized by a crystallization peak at 92.91 °C and a smaller exotherm (P_{exo}) at 154.75 °C prior to a single melting peak (P_1), which is placed at 168.82 °C. These values are somewhat smaller than those measured by the conventional DSC during the first heating scan (see Figure 7.1). However, they cannot be exactly compared because the heating rates used are not the same. Crystallization processes and the major part of melting are observed in the non-reversible curve. The reversing heat flow curve is characterized by two small endotherms, (Figure 7.10 (b), lowest), the first of which occurring simultaneously with the exotherm. This obeys the previously suggested melt-recrystallization model [15; 51; 56].

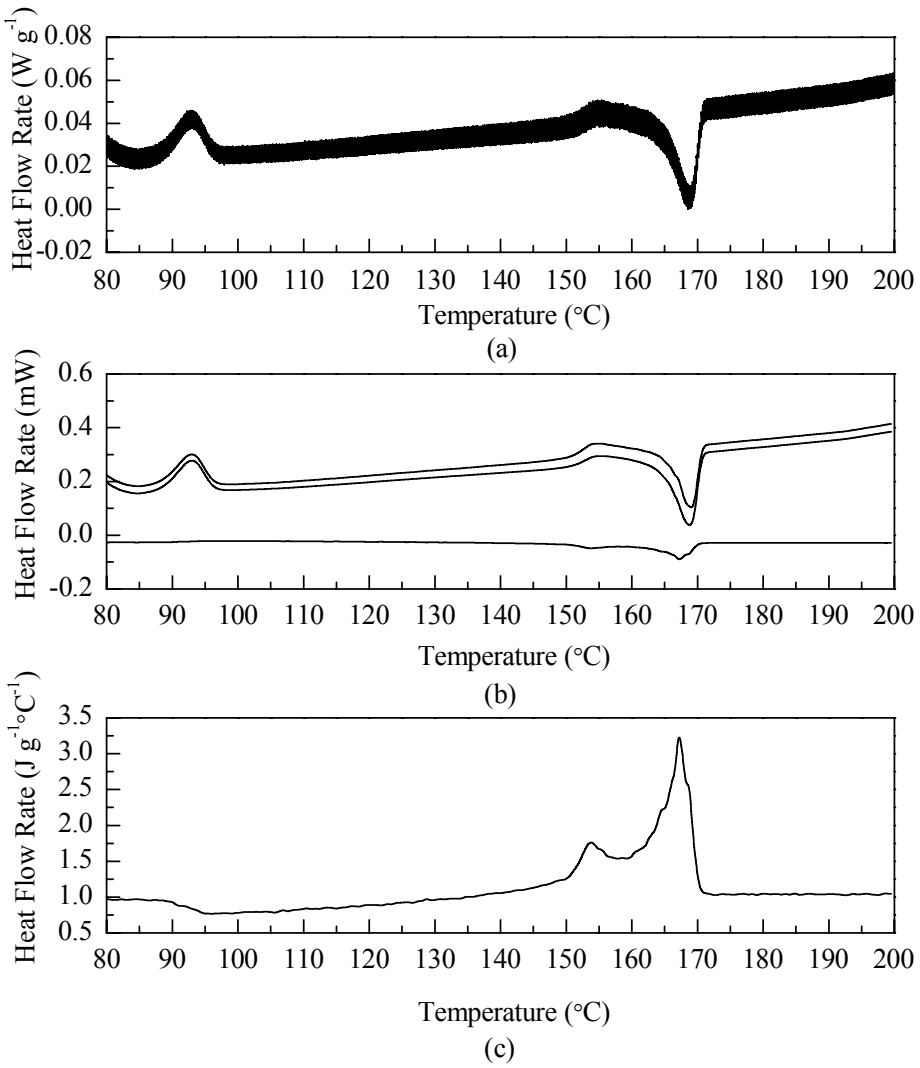

Figure 7.10 *The (a) measured heat flow of P(L/D)LA 99/1, from which the (b) non-reversing (upper), total (middle), and reversing heat flow (lower) curve alongside (c) quasi-static heat capacity curve are evaluated. The sample was not crystallized beforehand. The underlying heating rate was 0.25 °C min^{-1} and the pulse height was 0.05 °C. The width of the calculation window was 225 s.*

Next, the melting behavior of P(L/D)LA 99/1 was investigated by crystallizing the sample for one hour at the temperatures between 90 and 130 °C, after which the TOPEM measurement was performed. The peak temperatures of thermal events and the degrees of crystallinity are presented in Table 7.7. Corresponding curves are illustrated in Figure 7.11. At 90 °C < T_c < 100 °C, P_{exo} is observed prior to P_1. The second melting peak (P_2) is present, when T_c > 110 °C. These results are similar to those recorded with conventional DSC (see Table 7.2), except in this case P_2 distinguishes itself more clearly. Increasing of T_c shifts both endotherms to higher temperatures, but does not affect their magnitudes. Thus a conclusion can be drawn that in this case one hour is not sufficient for crystallization of P(L/D)LA 99/1. For this reason three hours of crystallization was carried out as well.

In addition to the different heat flow curves, the quasi-static heat capacity is obtained as well. From Figure 7.11 (d) it can be observed that the main part of heat capacity originates from P_1, but P_{exo} and P_2 give a rise to the small part as well.

Table 7.7 *The peak temperatures of crystallization (T_{exo}) and melting processes (T_{m1} and T_{m2}) observed in the total heat flow curve of P(L/D)LA 99/1 alongside the degrees of crystallinity (X). The sample was crystallized for one hour at various temperatures before TOPEM measurements.*

T_c (°C)	T_{exo} (°C)	T_{m2} (°C)	T_{m1} (°C)	X (%)
90	156.33	-	171.19	47.6
100	158.75	-	170.31	40.1
110	-	164.16	171.31	44.0
113	-	165.20	171.56	45.9
130	-	165.74	172.21	50.2

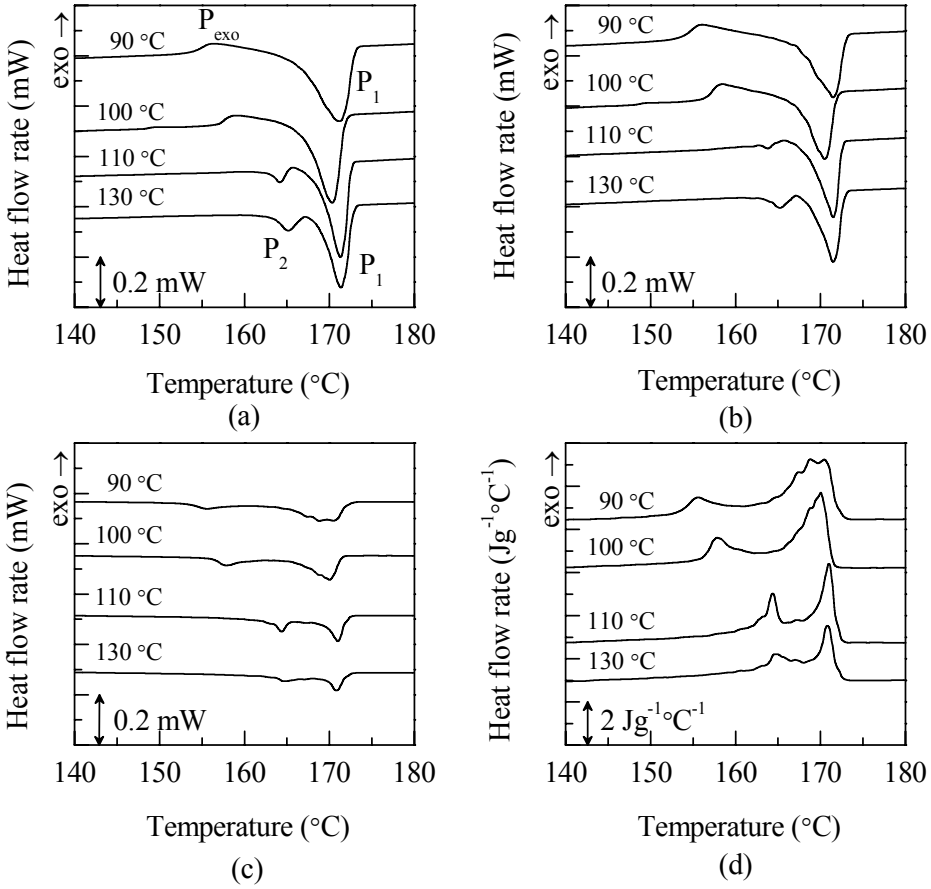

Figure 7.11 *TOPEM data of P(L/D)LA 99/1 predicting the curves of (a) the total heat flow, (b) non-reversing heat flow, (c) reversing heat flow, and (d) quasi-static heat capacity plotted against temperature. The sample was crystallized beforehand at various temperatures for one hour. The curves have been shifted vertically for clarity.*

The results of the TOPEM measurements performed after three hours of crystallization are shown in Table 7.8 and Figure 7.12. The crystallization temperature was between 90 and 140 °C.

Table 7.8 *The peak temperatures of cold crystallization (T_{cc}), the exotherm (T_{exo}), and two melting peaks (T_{m1} and T_{m2}) of the total heat flow curves alongside the degrees of crystallinity (X). The P(L/D)LA 99/1 sample was crystallized at various temperatures for three hours before the TOPEM measurements.*

T_c (°C)	T_{cc} (°C)	T_{m2} (°C)	T_{exo} (°C)	T_{m1} (°C)	X (%)
90	154.68	-	-	169.26	42.6
100	158.71	-	-	169.69	42.0
113	-	164.45	165.79	171.28	46.0
120	-	164.87	166.21	170.90	38.7
130	-	167.23	-	172.08	36.4
140	-	-	-	169.22	44.1

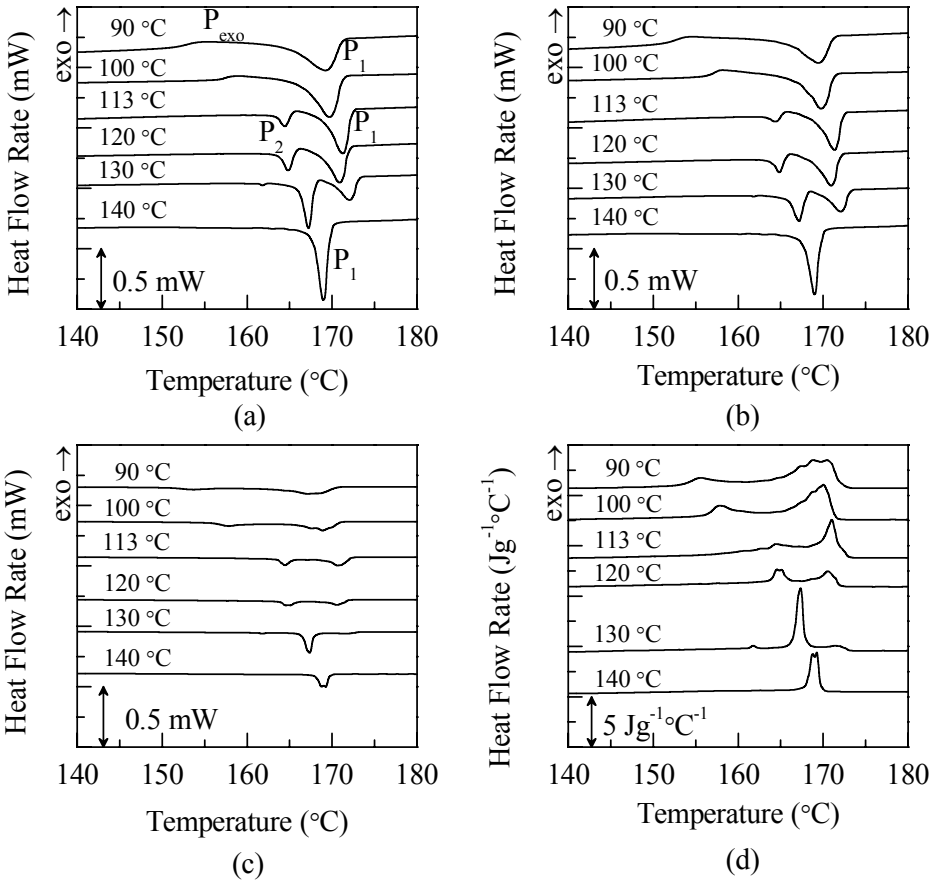

Figure 7.12 *The (a) total heat flow, (b) non-reversing heat flow, (c) reversing heat flow, and (d) quasi-static heat capacity curves of P(L/D)LA 99/1 measured after crystallization at various temperatures for three hours. The curves have been shifted vertically for clarity.*

In this case both endotherms are visible. The peak temperature of P_1 is slightly lower compared to that obtained after one hour of crystallization. The peaks shift and their areas change in a similar manner as in the case of the conventional DSC measurements. On the contrary, the non-reversing and reversing processes overlapping can now be separated. From Figure 7.11 and Figure 7.12 it can be observed that the crystallization peak appears in the non-reversing curve as well as the major part of the melting process. The reversing curves are characterized by two small endotherms. At $T_c \leq 100$ °C, the first endotherm is located at the same temperature as P_{exo} in the non-reversing curve.

7.2.4 TOPEM analysis of P(L/D)LA 96/4

Figure 7.13 shows the DSC curves of P(L/D)LA 96/4 obtained from a TOPEM measurement without preliminary crystallization.

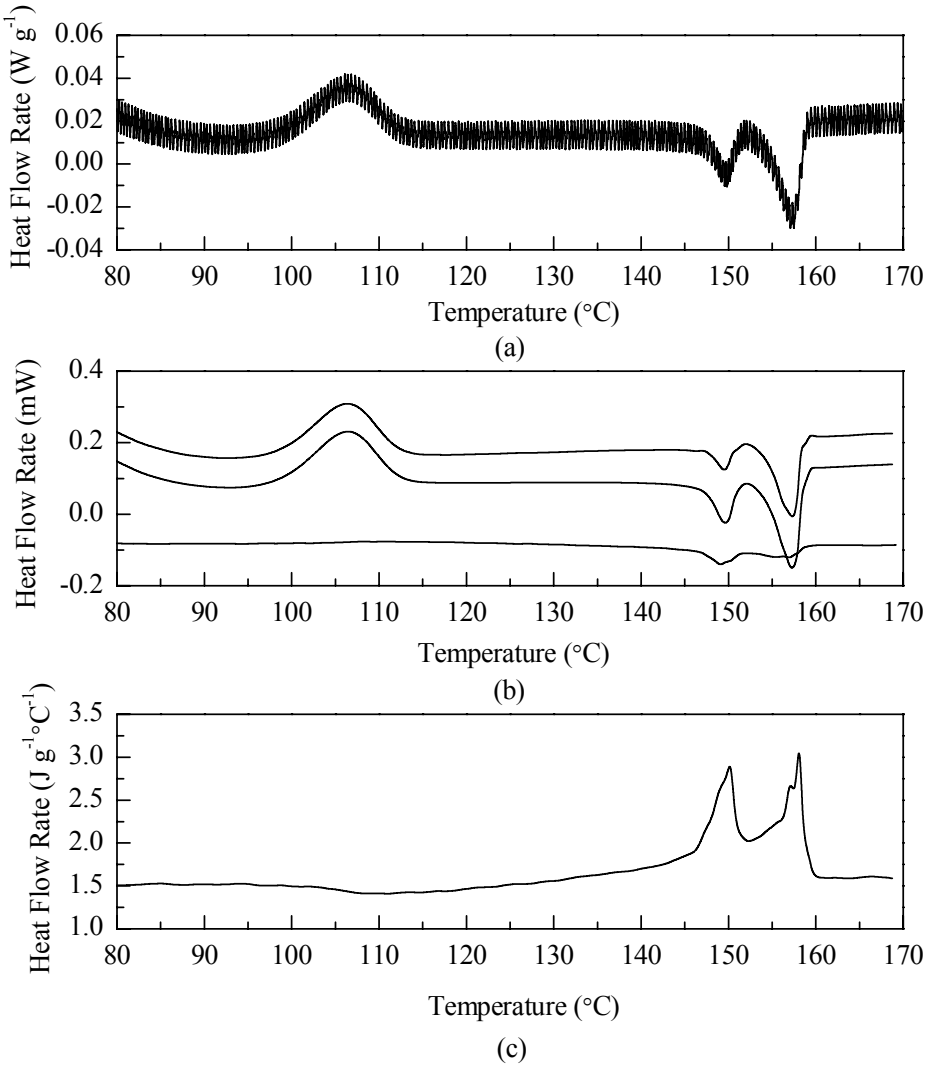

Figure 7.13 *The (a) measured heat flow of P(L/D)LA 96/4, from which the (b) non-reversing (upper), total (middle), and reversing heat flow (lower) curve alongside (c) quasi-static heat capacity curve are evaluated. The heating rate was 0.5 °C min^{-1}, the pulse height was 0.05 °C, and the width of the calculation window was 175 s.*

As in the case of P(L/D)LA 99/1, the total heat flow curve is characterized by crystallization and melting events. However, in this case an additional melting peak is present instead of P_{exo}. The cold-crystallization peak appears at 106.46 °C, which is somewhat higher than for P(L/D)LA 99/1. This is probably due to the faster heating rate. The peak P_1 is at 157.28 °C and P_2 is at 149.62 °C. The peak temperature of the first endotherm is slightly higher compared to the one of the first heating scan of the conventional DSC measurement, while the peak P_2 was not present in that study (Table 7.1). The P(L/D)LA 96/4 sample was crystallized for one hour at temperatures between 90 and 130 °C, after which the TOPEM measurement was performed. The peak temperatures of thermal events and the degrees of crystallinity are presented in Table 7.9. Corresponding curves are illustrated in Figure 7.14.

Table 7.9 *The peak temperatures of endotherms (T_{m1} and T_{m2}) observed in the total heat flow curve alongside the degrees of crystallinity (X). The P(L/D)LA 96/4 sample was crystallized at various temperatures for one hour before TOPEM measurements.*

T_c (°C)	T_{m1} (°C)	T_{m2} (°C)	X (%)
90	156.18	145.60	27.3
95	156.51	147.35	25.6
100	156.93	148.43	26.4
105	157.34	149.60	27.3
110	157.70	150.78	26.8
120	158.54	153.19	24.5
130	155.84	-	30.2

From Figure 7.14 it can be observed that the double melting behavior of the sample is similar as in conventional DSC studies, see Figure 7.2. The peak temperatures, however, are again higher in the case of TOPEM measurements. When T_c is 120–130 °C, the intensities of P_1 detected in the total and non-reversing heat flow curves are relatively high compared to the measurements performed at other temperatures. The quasi-static heat capacity seems to originate mainly from P_2, because it appears at the same temperature. This is different from the case of P(L/D)LA 99/1 (Figure 7.12 (d)), for which at T_c of 90–113 °C the main part of the quasi-static heat capacity originates from P_1. However, at $T_c \geq 120$ °C, the quasi-static heat capacity is due to P_2.

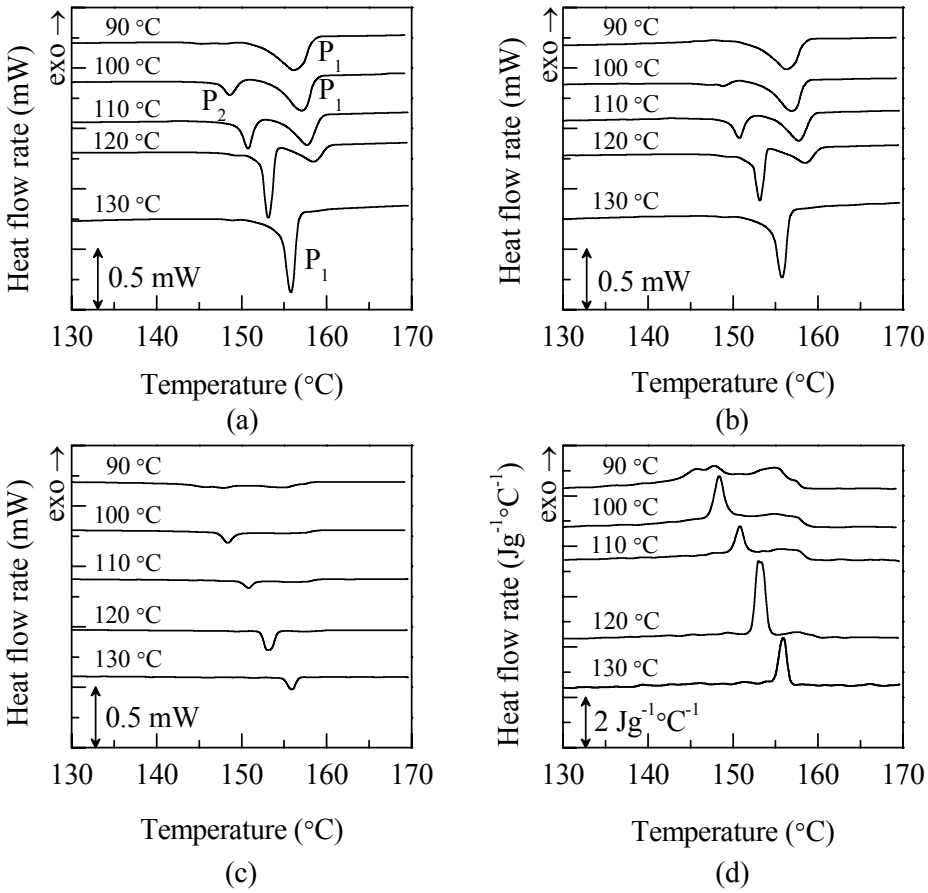

Figure 7.14 *The (a) total heat flow, (b) non-reversing heat flow, (c) reversing heat flow, and (d) quasi-static heat capacity curves of P(L/D)LA 96/4 obtained after one hour of crystallization. The curves have been shifted vertically for clarity.*

The characteristic values of thermal events detected on the total heat flow curve, when the sample was isothermally pre-crystallized for three hours, are presented in Table 7.10. The curves evaluated from the measured heat flow curve are shown in Figure 7.15.

Table 7.10 *The peak temperatures of melting and crystallization processes of P(L/D)LA 96/4 occurring in the total heat flow curve. The sample was crystallized for three hours at various temperatures before TOPEM measurements.*

T_c (°C)	T_{m1} (°C)	T_{exo} (°C)	T_m (°C)	X (%)
90	156.20	147.63	145.13	24.5
95	156.60	-	147.44	24.8
100	157.10	-	148.60	26.0
105	157.35	-	149.85	25.0
110	157.68	-	151.02	25.1
120	158.54	154.63	153.44	20.1
130	156.19	-	-	30.5

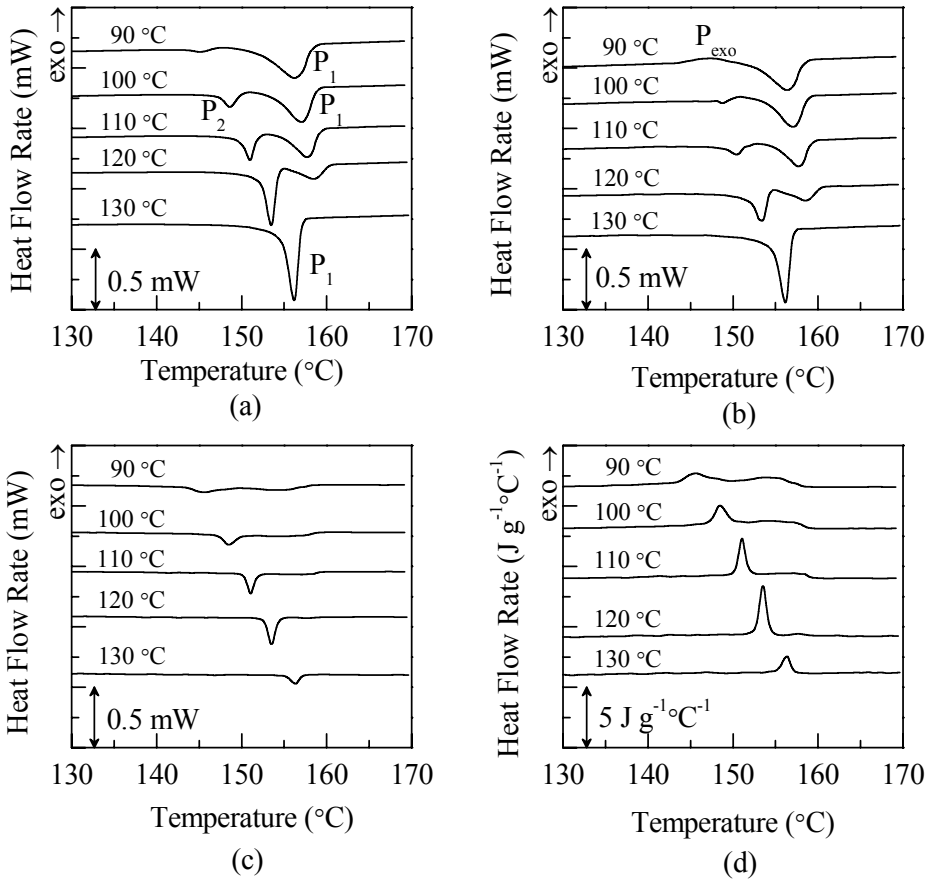

Figure 7.15 *The (a) total heat flow, (b) non-reversing heat flow, (c) reversing heat flow, and (d) quasi-static heat capacity curves of P(L/D)LA 96/4 obtained after three hours of crystallization at various temperatures. The curves have been shifted vertically for clarity.*

In all TOPEM measurements the major part of the melting and recrystallization processes was detected on the non-reversing heat flow curve, while the rest of melting appeared in the reversing heat flow curve. Shieh et al. attained similar results when studying PLLA by TMDSC with the underlying heating rate of 1 °C min^{-1}, the amplitude of 0.5 °C, and the period of 60 s. Their sample was reported to have a few percent of optical impurity but the exact content was not told. However, the peak temperatures they obtained with the conventional DSC are quite close to those of P(L/D)LA 99/1, which indicates that their sample had the impurity content of about 1%. The temperature range they used is narrower (100–110 °C) than the one used in this study. In this region the appearance of the exotherm and both endotherms are quite similar as in Figure 7.12. [16]

The non-reversing melting is usually observed when the melting of the sample is so slow that it does not occur in the equilibrium. One example of this is the melting of superheatable crystals. [77] Superheating behavior occurs, when the molecular rearrangement to the new phase is slowed or hindered [78]. This phenomenon explains also the shift of the melting peak to the higher temperature with faster heating rate [79]. Re-

versible melting in turn is suggested to be due to partial melting of lamellae, which is followed by rapid recrystallization. In the case of PET the reversible melting was also explained by molecular nucleation. [80; 81]

7.3 FTIR spectroscopy of PDLLA

The plasticizing effect of water on PDLLA was examined by FTIR spectrometer. The characteristic absorption bands of Film 1 measured after vacuum drying are presented in Table 7.11, where they are compared to the reference values. The full spectra of the film recorded from the dry and wet samples are shown in Figure 7.16. As for other cast films, the results were so similar that they are not presented here. The focus will only be on the bands, which undergo some changes caused by water and thermal treatment or by gamma sterilization.

Table 7.11 *Band assignments of amorphous PDLLA (Film 1) obtained after vacuum drying.*

Assignment	***υ* (cm^{-1})** **0 d (in water)**	**References**
ν_s(OH) (water)	3657	3652 [75]
ν(OH) free (PLA)	3565	3571 [82; 83]
2xν(C=O)	3505	3500 [4]
$\nu_{as}(CH_3)$	2995	2997 [82; 83]
$\nu_s(CH_3)$	2945	2947 [82]; 2946 [34]
ν(CH)	2881	2882 [82]; 2877 [34]
ν(C=O)	1765, 1758, 1754, 1748	1760 [82; 83]; 1748 [34]
δ (HOH)		1625 [84]; 1641 [85]
$\delta_{as}(CH_3)$	1454	1452 [82; 83]; 1456 [34]
$\delta_s(CH_3)$ [82] –CH– deformation including symmetric and asymmetricbend [34]	1382	1385 [82]; 1382 [34]
$\delta1(CH)+\delta_s(CH_3)$	1364	1365 [34; 82]
δ2(CH)	1320	1300, 1315 [82]
δ(CH)+ν (COC)	1269	1270 [82; 83]
ν_{as}(COC) (+ $r_{as}(CH_3)$ [83])	1187	1185 [82]
$r_{as}(CH_3)$	1131	1130 [82; 83]
ν_s(COC)	1094	1090 [82]; 1093 [34]
ν(C-CH_3)	1051	1045 [82; 83]
r(CH_3)+ν(CC)	956	960 [82]; 956 [34]
ν(C-C)	866	868 [34]
δ(C=O)	752	760 [82]
δ_1C-CH_3 + δCCO	516	515 [82]

The bands at 2997, 2946 and 2877 cm^{-1} are due to the CH stretching modes. A very strong band splitted in several peaks, which are observed at 1765, 1758, 1754 and 1748 cm^{-1}, is assigned to the C=O stretching mode. Other general bands for PLA-based polymers are asymmetric stretching of CH_3 at 1454 cm^{-1}, symmetric bending of CH_3 at 1382 cm^{-1}, and the C-O-C stretching modes at 1187 and 1094 cm^{-1}. The band at 956 cm^{-1} is related to the helical backbone vibrations, that is, to the CH_3 rocking modes.

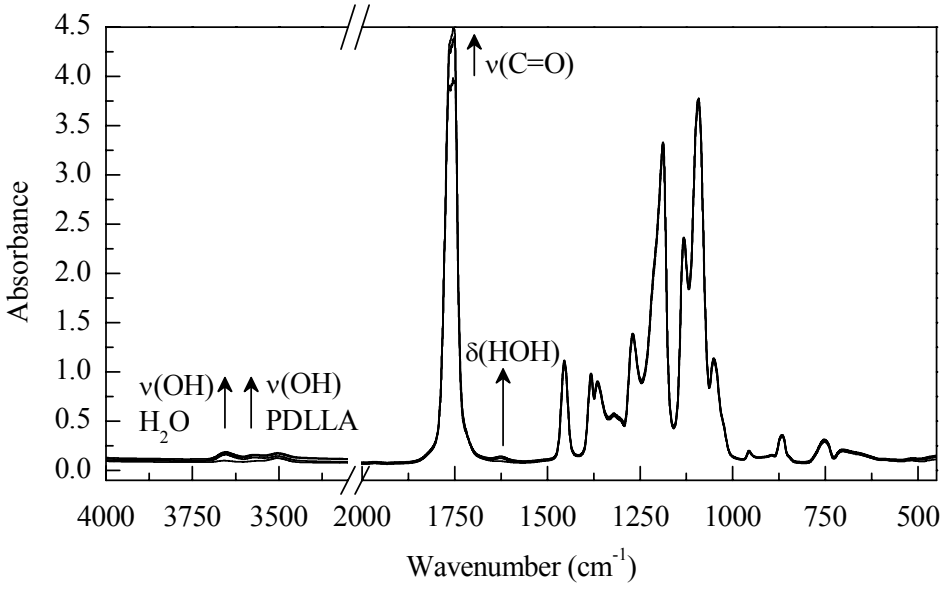

Figure 7.16 *FTIR spectra of a PDLLA sample (Film 1) immediately after drying in vacuum and after exposing to water at 37 °C for one, two, and seven days. The changes in the spectra are marked with the arrows, which show the direction of the intensity changes during water treatment.*

Arrows indicate the direction of intensity changes during water treatment in the areas of interest for this study. Particular attention is paid to the region of 3900–3300 cm^{-1}, where the effect of water is clearly seen. Another subject of interest is the band appearing to the right side of the carbonyl peak due to the water exposure. The intensity of the C=O stretching mode is changing, as well. A closer look at the effect of water on films with different treatments is given in the next subsections.

7.3.1 Water treatment of PDLLA with intermediate measurements

Both Film 1 and Film 4 were exposed to water at 37 °C and measured at certain intervals. In addition, Film 4 was gamma sterilized before water treatment. Table 7.12 shows the band assignments of Film 1 obtained during the experiment in the regions defined in Figure 7.16. The changes observed are the most significant during the first day, after which the shifts observed are smaller. The symmetric stretching of the OH group of water moves from 3657 to 3652 cm^{-1}. Also, the free ν(OH) stretching originating from the polymer itself moves to higher wavenumber. This indicates that the increasing

amount of water absorbed by film degrades the polymer via hydrolysis, which results in the greater amount of free hydroxyl groups. The third band, which is associated with an overtone of ν(C=O) vibrations in the range of 1765–1748 cm^{-1}, occurs at 3505 cm^{-1}. After water immersion it shifts only slightly to lower wavenumber and stays unaltered during the rest of the experiment. A new weak band appearing next to the carbonyl peak at 1626 cm^{-1} is assigned to the H-O-H bending of water.

Table 7.12 *The band assignments of Film 1 after vacuum drying (0 d) and after exposing to water for various time periods between measurements.*

Assignment	**0 d (in water)**	**1 d (in water)**	**2 d (in water)**	**7 d (in water)**
ν_s(OH) (water)	3657	3653	3653	3652
ν(OH) free (PLA)	3565	3568	3569	3569
2xν(C=O)	3505	3504	3504	3504
ν(C=O)	1765, 1758, 1754, 1748	1764, 1762, 1758, 1754, 1750	1764, 1762, 1758, 1754, 1749	1761, 1753, 1750
δ(H-O-H)	-	1626	1625	1625

The band assignments of Film 4 are presented in Table 7.13. In order to examine the effect of sterilization on the dry film, it was also measured before gamma sterilization, immediately after preparation. However, these two cases are not totally comparable, because the film was not vacuum dried after preparation, for which reason there can be some traces of acetone or water in the spectrum. After gamma sterilization the ν_s(OH) of water has shifted from 3652 to 3657 cm^{-1}, which is exactly the same wavenumber observed for Film 1 after vacuum drying. Based on this information it is difficult to say, whether this shift is due to gamma sterilization or vacuum drying. The ν(OH) mode of PLA is barely visible in the dry sample at 3554 cm^{-1} and after seven days of water immersion it occurs at 3568 cm^{-1}. The overtone of *ν*(C=O) in turn occurs at 3509 cm^{-1}, which is higher compared to Film 1. During water treatment the band shifts to 3505 cm^{-1}.

Table 7.13 *The band assignments of Film 4 after preparation and gamma sterilization followed by water immersion for various time periods.*

Assignment	**0 d (after preparation)**	**0 d (after γ-sterilization)**	**1 d (in water)**	**2 d (in water)**	**7 d (in water)**
ν_s(OH) (water)	3652	3657	3652	3655	3651
ν(OH) (free PLA)	3554	3554	3568	3569	3568
2xν(C=O)	3509	3508	3506	3505	3505
ν(C=O)	1762, 1753, 1712	1750, 1706	1754, 1749	1758, 1754, 1749	1758, 1754, 1749
δ(H-O-H)	-	-	1628		1629

From the Figure 7.17 it can be observed that the FTIR spectra of dry Film 1 and 4 differ greatly from each other. In the Film 1 three bands are more easily distinguishable than in the case of Film 4. After water immersion both films show similar behavior: intensity of the ν_s(OH) mode of water increases significantly. The intensity of the stretching mode of free hydroxyl groups increases as well, but not to the same extent. Intensity of the third band (the overtone of ν(C=O)) hardly changes for Film 1. On the contrary, this difference is much greater in the spectra of Film 4. During the water immersion the third band is easily detected, while in the spectrum of the dry sample it appears as one broad band with a shoulder.

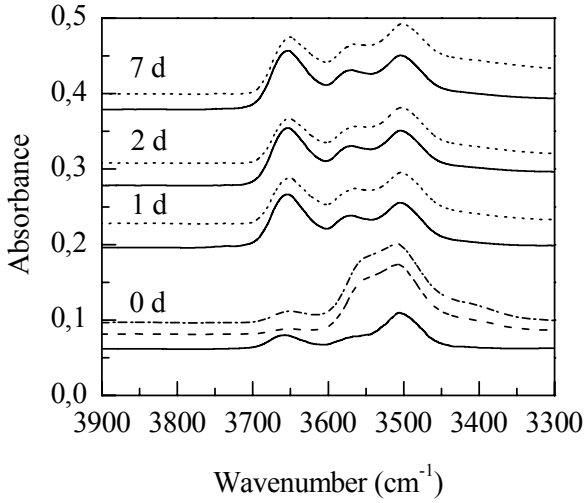

Figure 7.17 *FTIR spectra of Film 1(solid lines) and Film 4 (dotted lines) in the region between 3900 and 3300 cm^{-1} before and after water treatment of one, two, and seven days. The spectrum of Film 1 after drying it in vacuum (the lowest line) was used as a reference for normalization. The dash dotted line presents the Film 4 before gamma sterilization and the dashed line under it the same film after gamma sterilization but before exposure to water. The curves have been shifted vertically for clarity.*

Figure 7.18 (a) and (c) present the spectra of Film 1 and 4 in the C=O stretching region, respectively. In both cases the positions of the peaks stay unaltered. Their intensities change during the experiment, but there is no regularity. Especially, in the case of Film 4 the changes seem to be coincidental. However, in Figure 7.18 (d), where the formation of the H-O-H band is shown, the direction of the changes is completely different. The H-O-H mode of Film 1 is illustrated in Figure 7.18 (b). Apart from the higher intensity of the peak in the spectra of Film 1 there are no significant differences between these two films.

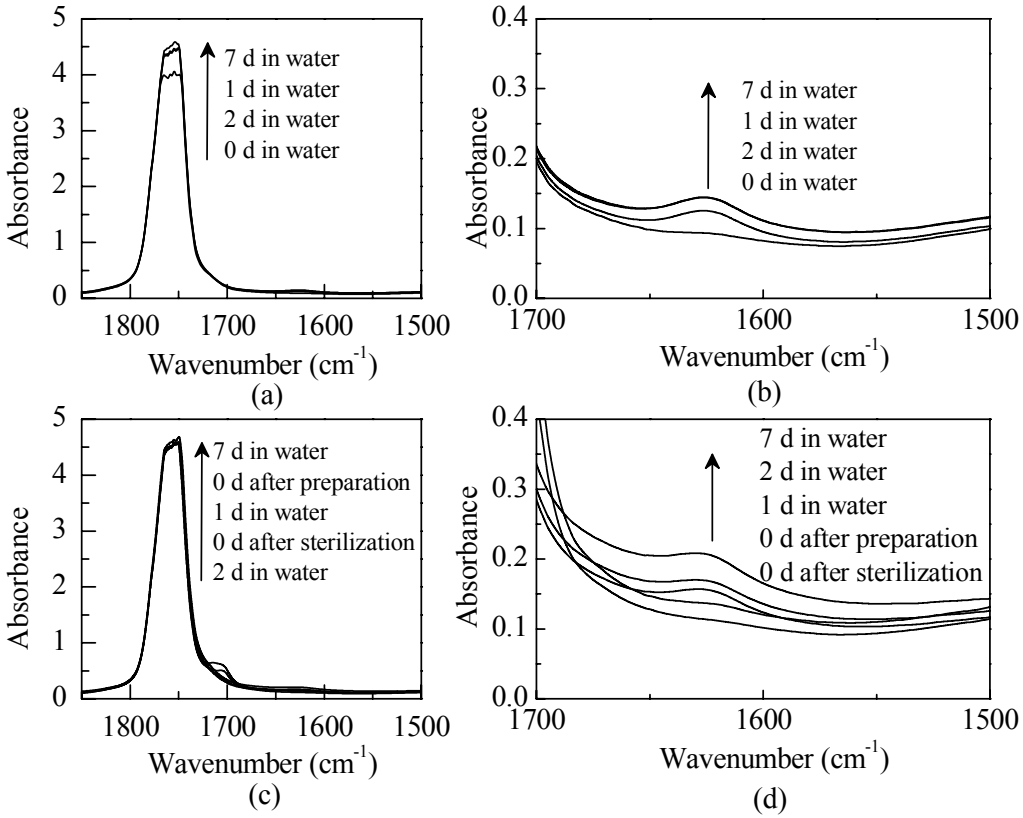

Figure 7.18 *The spectra of Film 1 in the region of (a) 1850–1500 cm^{-1} and (b) 1700-1500 cm^{-1} alongside the spectra of Film 4 in the region of (c) 1850–1500 cm^{-1} and (d) 1700–1500 cm^{-1}.*

From Figure 7.18 (a) and (b) one can also observe that the C=O stretching band splits into several peaks. This phenomenon is proposed to be due to the intramolecular coupling. Other explanation given is the interchain interactions, such as C-H···O hydrogen bonding or dipole-dipole interaction, but the origin has not been confirmed yet. [82]

7.3.2 Water treatment of PDLLA without intermediate measurements

Film 2 and 5 were also exposed to water, but in this time no intermediate measurements were performed. Film 2 was analyzed only two times: after vacuum drying and seven days of immersion. The measured band assignments of Film 2 are presented in Table 7.14. The effect of water is very similar to that of Film 1. The ν_s(OH) mode of water shifts to lower wavenumber. The OH stretching mode of free hydroxyl groups of polymer cannot be observed right after drying but it appears during immersion and is placed at 3569 cm^{-1}. The overtone of the carbonyl appears at 3505 cm^{-1} and there are no significant changes in it during the experiment. The ν(C=O) stretching mode stays about at the same wavenumber as well. The H-O-H bending mode of water appears at 1626 cm^{-1} after water immersion.

Table 7.14 *Band assignments of Film 2 after vacuum drying and exposing it to water for seven days without intermediate measurements.*

Assignment	**0 d (in water)**	**7 d (in water)**
ν_s(OH) (water)	3656	3652
ν(OH) free (PLA)	3564	3569
2x ν (C=O)	3505	3504
ν(C=O)	1765, 1763, 1758, 1754, 1750, 1747	1765, 1762, 1758, 1754, 1750, 1747
δ (H-O-H)	-	1626

Film 5 was gamma sterilized before vacuum drying and water treatment. Measured band assignments are presented in Table 7.15. As in the case of Film 2, gamma sterilization shift bands to higher wavenumbers. Especially ν_s(OH) of water, which shifts from 3650 to 3639 cm^{-1}. However, after water treatment it is replaced at 3651 cm^{-1}.

Table 7.15 *Band assignments of Film 5 after preparation and gamma sterilization, alongside water treatment for seven days without intermediate measurements.*

Assignment	**0d (after preparation)**	**0 d (after γ-sterilization)**	**7 d (in water)**
ν_s(OH) (water)	3650	3639	3651
ν(OH) free (PLA)	3552	3550	3567
2x ν (C=O)	3509	3507	3505
ν(C=O)	1756	1756	1756
δ(H-O-H)	-	-	1636

Figure 7.19 and Figure 7.20 illustrate both Film 2 and Film 5 before and after water treatment in the regions of 3900–3300 cm^{-1} and 1850–1500 cm^{-1}. All spectra were normalized by using dry Film 1 as reference. The intensities of the bands measured for Film 5 are so small compared to Film 2 that any changes are difficult to see. Figure 7.20 (b) and (d) present the δ (H-O-H) band in the region of 1700–1500 cm^{-1}.

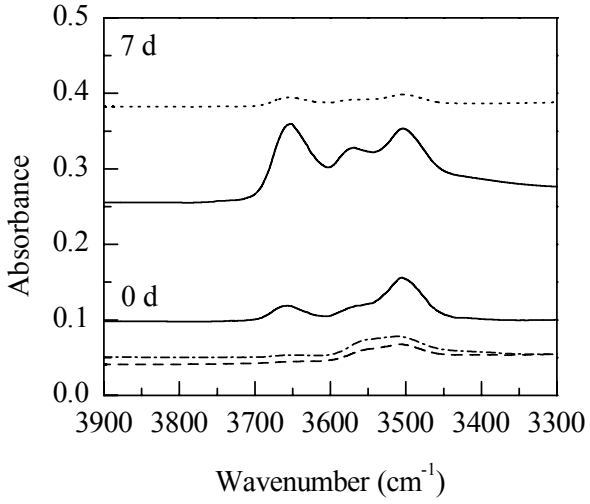

Figure 7.19 *FTIR spectra of Film 2 (solid lines) and Film 5 (dotted lines) in the region of 3900-3300 cm^{-1} before and after exposure to water for seven days. The dash dotted line presents the Film 5 before gamma sterilization and the dashed line under it the same film after gamma sterilization but before exposure to water. Curves have been shifted vertically for clarity.*

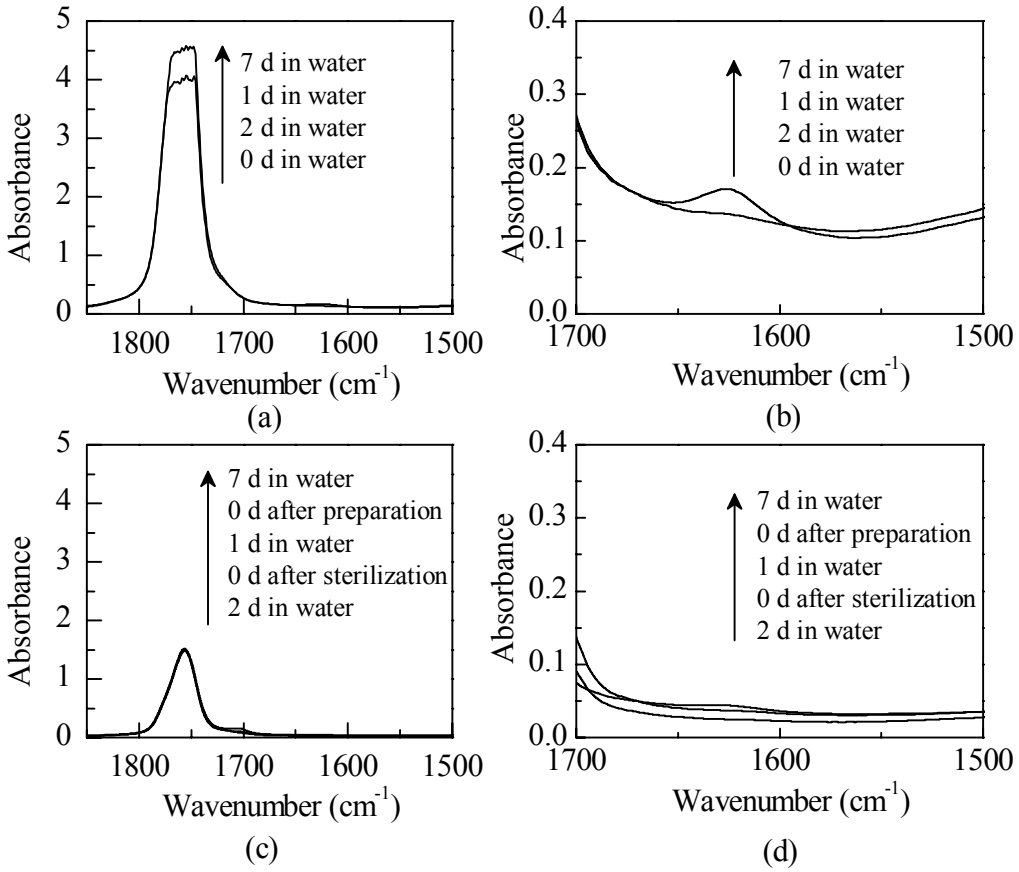

Figure 7.20 *The FTIR spectra of Film 2 in the region of (a) 1850–1500 cm^{-1} and (b) 1700-1500 cm^{-1} alongside the spectra of Film 5 in the region of (c) 1850–1500 cm^{-1} and (d) 1700–1500 cm^{-1}.*

The ν(C=O) band of Film 2 is splitting in a similar way as that of Film 1. In this case peaks distinguish themselves more clearly. In the case of Film 5 the band does not split. Figures 7.20 (b) and (d) shows that the appearance of the H-O-H bending mode during water treatment proceeds in the same manner than above.

The results obtained from the water immersion experiments show that the infrared band of C=O stretching did not shift during experiment. This indicates that no hydrogen bonds were formed between the polymer and water molecules [85]. However, from the IR spectra illustrated above it can be concluded that water has some effect on it. The increase of the ν(C=O) overtone band during immersion might be caused by degradation of the polymer, because the carbonyl groups have more space for vibration in the monomers than in the polymer. This could also explain the intensity changes in the ν(C=O) band.

7.3.3 Thermal treatment of PDLLA with intermediate measurements

In the third procedure films (Film 3 and Film 6) were kept in the drying oven at the temperature of 37 °C without exposure to water. This was done to measure the effect of thermal treatment on the samples. The band assignments measured for Film 3 after drying and during thermal treatment for one, two, and seven days are shown in Table 7.16. The only peak shifting is ν_s(OH) of water. It moves to higher wavenumber. The ν(OH) band of free hydroxyl groups of polymer shift from 3566 to 3569 cm^{-1} and stays unaltered during the rest of thermal treatment. The overtone of the carbonyl peak can be found at 3505 cm^{-1}. The H-O-H bending mode of water is absent as can be expected for a dry sample.

Table 7.16 *The band assignments measured for Film 3 after vacuum drying and keeping it in the drying oven at 37 °C without water treatment for various time periods.*

Assignment	**0 d (in the oven)**	**1 d (in the oven)**	**2 d (in the oven)**	**7 d (in the oven)**
ν_s(OH) (water)	3657	3658	3661	3660
ν(OH) free (PLA)	3566	3569	3569	3569
2x ν(C=O)	3506	3504	3505	3505
ν(C=O)	1756	1756	1756	1756

The band assignments for the FTIR spectra of Film 6 are presented in Table 7.17. The symmetric stretching of OH group arousing from water shifts to higher wavenumber. After seven days of thermal treatment it is located at 3658 cm^{-1}. As in the case of Film 3 the δ(H-O-H) mode of water is absent.

Spectra of Film 3 and Film 6 in the region of 3900–3300 cm^{-1} are shown in Figure 7.21. Thermal treatment decreases intensities of the bands linearly. The band intensities of the gamma sterilized sample are lower than for untreated one. In the FTIR spectra of Film 3 and 6 no splitting of the ν(C=O) band was observed and for that reason this region is not illustrated here.

Table 7.17 *Band assignments of Film 6 observed after preparation, after gamma sterilization, and during thermal treatment for various times.*

Assignment	0 d (after preparation)	0 d (after γ-sterilization)	1 d (in the oven)	2 d (in the oven)	7 d (in the oven)
ν_s(OH) (water)	3653	3660	3657	3661	3658
ν(OH) free (PLA)	3547	3546	3547	3547	3547
2x ν (C=O)	3510	3508	3507	3507	3507
ν(C=O)	1756	1756	1756	1756	1756

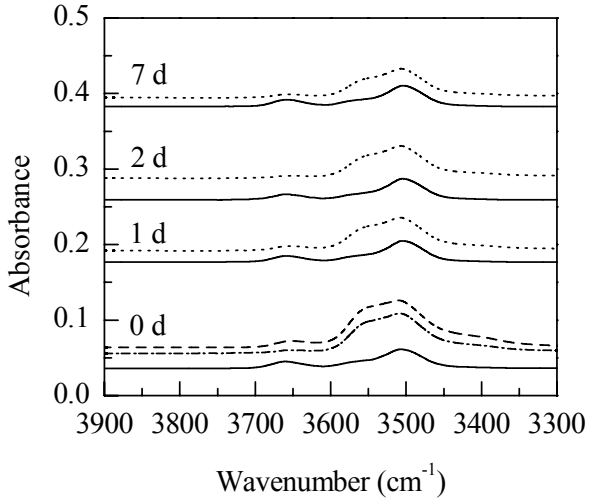

Figure 7.21 *FTIR spectra of Film 3 (solid lines) and Film 6 (dotted lines) in the region of 3900–3300 cm^{-1} before and after thermal treatment for seven days. The dash dotted line presents the Film 6 before gamma sterilization and the dashed line under it the same film after gamma sterilization but before exposure to water. The spectra have been shifted vertically for clarity.*

Overall, there was no clear evidence of the effect of gamma sterilization on the cast films. The positions of the absorption bands alter slightly during the treatment, but as stated before, this might be also due to vacuum drying. The intensities of the bands stay unchanged. The strangely broad overtone band detected for dry Film 4–6 complicated the interpretation of the spectra. The reason for the appearance of it is unclear, but it might somehow be due to poorer quality of films. After the water immersion two separate bands are distinguishable at the place of the band. Otherwise, the spectra of unsterilized and sterilized films measured after water immersion resemble each other closely, and the effect of water can be clearly seen there.

8 SUMMARY

In this thesis the double melting behavior of poly(lactic acid) was investigated by the new TMDSC method, TOPEM. The purpose of the study was to determine the suitable parameters for examination of the melting processes of this particular polymer and find out, whether the TOPEM technique would offer some new insights about this widely investigated phenomenon. The results obtained were compared with the ones derived by conventional DSC studies. Additionally, the plasticizing effect of water on the untreated and gamma sterilized PLA samples were studied by FTIR. Semicrystalline PLAs with D-content of 1 and 4% were used as sample materials for TOPEM measurements, whereas in FTIR studies the material investigated was medical grade PDLLA, which was a completely amorphous polymer.

Conventional DSC studies were performed before TOPEM experiments in order to clarify the behavior of the samples. Crystallization times of one and three hours were compared. It was found out that the PLA sample with higher L-content required longer crystallization time for the appearance of the second melting peak. The temperature range, where two endotherms were visible, took place at lower temperatures for P(L/D)LA 96/4 than for P(L/D)LA 99/1. This was explained by different D-content of the samples.

The suitable parameters for TOPEM studies were determined by preliminary studies. Different heating rates and pulse heights were tested. The results indicated that the PLA with higher L-content required slower heating rate in order to prevent noisy and possible wrong results. Thus, the heating rate chosen for P(L/D)LA 99/1 was 0.25 °C min^{-1}, while the heating rate of 0.5 °C min^{-1} was used for P(L/D)LA 96/4. The pulse height of 0.05 °C was used for both samples. The effect of the calculation window width was also studied by comparing the total heat flow curve to the mean value of measured heat flow curve. The calculation windows of 225 and 175 s were chosen for P(L/D)LA 99/1 and 96/4, respectively.

The TOPEM measurements correlated quite well with the conventional studies. They could not be exactly compared, because the heating rates used were not the same. This might explain the higher peak temperatures observed by TOPEM. The non-reversing and reversing heat flow curves of both samples showed that the melting and crystallization processes occurred simultaneously when using lower crystallization temperatures (T_c < 100 °C). At higher temperatures the double melting peaks were observed as in the case of the conventional DSC studies. The melting processes of both samples were detected to be mainly irreversible. The reason for this might be superheating of the samples due to the slow melting kinetics of them.

So far the main focus of TOPEM studies has been in the glass transition region. The results obtained in this study give more information about the examination of melting processes by TOPEM. It was shown that it is possible to detect the double melting behavior of PLA with this method. Also, more information about the effect of different D-contents on this phenomenon was gained.

The cast films made of PDLLA were investigated by FTIR. They were exposed to water for various time periods in order to study its plasticizing effect. Films were measured by transmission technique. The most significant changes in the FTIR spectra were observed in the region of 3700-3500 cm^{-1}, where three absorption bands were detected. They were assigned to the ν_s(OH) mode of water, ν(OH) mode of the polymer and the overtone of the carbonyl peak. The changes in these bands were suggested to be due to degradation of PLA via hydrolysis, in which case the amount of hydroxyl chain ends would increase. Increasing intensity of the overtone band was explained by increasing degree of freedom of carbonyl group. Additionally, a new band appeared on the right side of ν(C=O) in the region of 1650–1600 cm^{-1} during water treatment. This was assigned to the δ(H-O-H) mode of free water.

The results attained during immersion were compared to the sample kept in the oven at the same temperature. In this case no significant changes in wavenumbers and intensities were observed. The effect of gamma sterilization on the samples was examined as well. However, no clear evidence of it was attained. Only slight changes in the wavenumbers of the absorption bands were observed, but this can be also due to the vacuum drying. Another reason for this might be poorer quality of the films, which were gamma sterilized. Too broad overtone band complicated the interpretation of their spectra.

The FTIR study offered very valuable information about the plasticizing effect of water on the amorphous PDLLA. However, additional studies are required to clarify the real effect of gamma sterilization. For this, the preparation method of cast films should be improved in such manner that the variation between the sample thicknesses would be smaller.

REFERENCES

[1] Lim, L.T., Auras, R. & Rubino, M. Processing technologies for poly(lactic acid). Progress in Polymer Science. 33(2008)8, pp. 820–852.

[2] Garlotta, D.A Literature Review of Poly(Lactic Acid). Journal of Polymers and the Environment. 9(2001)2, pp. 63–84.

[3] Zhang, J., Tashiro, K., Tsuji, H. & Domb, A.J. Disorder-to-Order Phase Transition and Multiple Melting Behavior of Poly(l-lactide) Investigated by Simultaneous Measurements of WAXD and DSC. Macromolecules. 41(2008)4, pp. 1352–1357.

[4] Zhang, J., Duan, Y., Sato, H., Tsuji, H., Noda, I., Yan, S. & Ozaki, Y. Crystal Modifications and Thermal Behavior of Poly(l-lactic acid) Revealed by Infrared Spectroscopy. Macromolecules. 38(2005)19, pp. 8012–8021.

[5] Niaounakis, M., Kontou, E. & Xanthis, M. Effects of aging on the thermomechanical properties of poly(lactic acid). Journal of Applied Polymer Science. 119(2011)1, pp. 472–481.

[6] Haines, P.J. Principles of thermal analysis and calorimetry. 2002, Royal Society of Chemistry. 220 p.

[7] Gill, P., Sauerbrunn, S. & Reading, M. Modulated differential scanning calorimetry. Journal of Thermal Analysis and Calorimetry. 40(1993)3, pp. 931–939.

[8] Reading, M., Elliott, D. & Hill, V. A new approach to the calorimetric investigation of physical and chemical transitions. Journal of Thermal Analysis and Calorimetry. 40(1993)3, pp. 949–955.

[9] Temperature Modulated DSC/ADSC. Annual STK Meeting, Greifensee, Switzerland, November 6, 2002. Mettler Toledo.

[10] Schawe, J. E. K. TOPEM® - the latest innovation in temperature modulated DSC The 16th Symposium on Thermophysical Properties, Boulder, CO, USA, July 30-August 4, 2006. Mettler Toledo.

[11] Wunderlich, B. Thermal analysis of polymeric materials. The Netherlands 2005, Springer. 894 p.

[12] TOPEM® - the new advanced multi-frequency TMDSC technique. Mettler Toledo. 8(2005), 8 p.

[13] Schawe, J. Analysis of melting processes using TOPEM®. Mettler Toledo UserCom. 25(2007)1, pp. 13–17.

[14] Kawai, T., Rahman, N., Matsuba, G., Nishida, K., Kanaya, T., Nakano, M., Okamoto, H., Kawada, J., Usuki, A., Honma, N., Nakajima, K. & Matsuda, M. Crystallization and Melting Behavior of Poly (l-lactic Acid). Macromolecules. 40(2007)26, pp. 9463–9469.

[15] Pan, P., Kai, W., Zhu, B., Dong, T. & Inoue, Y. Polymorphous Crystallization and Multiple Melting Behavior of Poly(l-lactide): Molecular Weight Dependence. Macromolecules. 40(2007)19, pp. 6898–6905.

[16] Shieh, Y.-T. & Liu, G.-L. Temperature-modulated differential scanning calorimetry studies on the origin of double melting peaks in isothermally melt-crystallized poly(L-lactic acid). Journal of Polymer Science Part B: Polymer Physics. 45(2007)4, pp. 466–474.

[17] Shen, C., Wang, Y., Li, M. & Hu, D. Crystal modifications and multiple melting behavior of poly(L-lactic acid-co-D-lactic acid). Journal of Polymer Science Part B: Polymer Physics. 49(2011)6, pp. 409–413.

[18] Smith, B. C. Introduction to Infrared Spectroscopy. In: Smith, B. C. Fundamentals of Fourier Transform Infrared Spectroscopy. Boca Raton 2011, CRC Press. pp. 1–17.

[19] Paakinaho, K., Heino, H., Pelto, M., Hannula, M., Törmälä, P. & Kellomäki, M. Programmed water-induced shape-memory of bioabsorbable polyD,L-lactide): activation and properties in physiological temperature. Journal of Materials Science: Materials in Medicine. 23(2012)3, pp. 613–621.

[20] Blasi, P., D'Souza, S.S., Selmin, F. & DeLuca, P.P. Plasticizing effect of water on poly(lactide-co-glycolide). Journal of Controlled Release. 108(2005)1, pp. 1–9.

[21] Engel, T. & Reid, P. J. Physical chemistry. San Francisco 2006, Pearson Benjamin Cummings. 1061 p.

[22] Widmann, G. & Riesen, R. Thermal analysis: terms, methods, applications. Heidelberg, Germany 1987, Dr. Alfred Hüthig Verlag GmbH. 131 p.

[23] Brown, E. M. Handbook of thermal analysis and calorimetry. Vol. 1. Principles and Practice. Amsterdam 1998, Elsevier Science B.V. 691 p.

[24] Zumdahl, S. S. Chemical principles. Boston 2005, Houghton Mifflin Company. 1164 p.

[25] Callister, W. D. Materials science and engineering: an introduction. New York 2007, John Wiley & Sons. 721 p.

[26] Braun, D., Cherdron, H., Rehahn, M. & Ritter, H. Polymer synthesis: theory and practice : fundamentals, methods, experiments. Berlin 2005, Springer. 385 p.

[27] Fried, J. R. Polymer science and technology. New Jersey 2003, Prentice Hall Professional Technical Reference. 582 p.

[28] Cowie, J. M. G. & Arrighi, V. Polymers: Chemistry and Physics of Modern Materials. Boca Raton 2007, CRC Press. 520 p.

[29] Nicholson, J. W. The Chemistry of Polymers. Dorset 2011, The Royal Society of Chemistry. 177 p.

[30] Henton, D.E., Gruber, P., Lunt, J. & Randall, J. Polylactic acid technology. In: Mohanty, A.K., Misra, M., and Drzal, L.T. (ed.). Natural fibers, biopolymers, and biocomposites. Boca Raton, USA 2005, Taylor & Francis Group, LLC. pp. 527–577.

[31] Fambri, L. & Migliaresi, C. Crystallization and Thermal Properties. In: Auras, R. A., Lim, L-T., Selke, S.E.M., Tsuji, H. (ed.). Poly(lactic acid): Synthesis, Structures, Properties, Processing, and Applications. New Jersey 2010, John Wiley & Sons, Inc. pp. 113–124.

[32] Groot, W., van Krieken, J., Sliekersl, O. & de Vos, S. Production and Purification of Lactic Acid and Lactide. In: Auras, R. A., Lim, L-T., Selke, S.E.M., Tsuji, H. (ed.). Poly(lactic acid): Synthesis, Structures, Properties, Processing, and Applications. New Jersey 2010, John Wiley & Sons, Inc. pp. 1–18.

[33] Clayden, J., Greeves, N., Warren, S. & Wothers, P. Organic Chemistry. New York 2001, Oxford University Press Inc. p. 1508.

[34] Auras, R., Harte, B. & Selke, S. An Overview of Polylactides as Packaging Materials. Macromolecular Bioscience. 4(2004)9, pp. 835–864.

[35] Sasaki, S. & Asakura, T. Helix Distortion and Crystal Structure of the α-Form of Poly(l-lactide). Macromolecules. 36(2003)22, pp. 8385–8390.

[36] Wasanasuk, K., Tashiro, K., Hanesaka, M., Ohhara, T., Kurihara, K., Kuroki, R., Tamada, T., Ozeki, T. & Kanamoto, T. Crystal Structure Analysis of Poly(l-lactic Acid) α Form On the basis of the 2-Dimensional Wide-Angle Synchrotron X-ray and Neutron Diffraction Measurements. Macromolecules. 44(2011)16, pp. 6441–6452.

[37] Wasanasuk, K. & Tashiro, K. Crystal structure and disorder in Poly(l-lactic acid) δ form (α′ form) and the phase transition mechanism to the ordered α form. Polymer. 52(2011)26, pp. 6097–6109.

[38] Puiggali, J., Ikada, Y., Tsuji, H., Cartier, L., Okihara, T. & Lotz, B. The frustrated structure of poly(l-lactide). Polymer. 41(2000)25, pp. 8921–8930.

[39] Hoogsteen, W., Postema, A. R., Pennings, A. J., Ten Brinke, G. & Zugenmaier, P. Crystal structure, conformation and morphology of solution-spun poly(L-lactide) fibers. Macromolecules. 23(1990)2, pp. 634–642.

[40] Cartier, L., Okihara, T., Ikada, Y., Tsuji, H., Puiggali, J. & Lotz, B. Epitaxial crystallization and crystalline polymorphism of polylactides. Polymer. 41(2000)25, pp. 8909–8919.

[41] Lunt, J. Large-scale production, properties and commercial applications of polylactic acid polymers. Polymer Degradation and Stability. 59(1998)1–3, pp. 145–152.

[42] Södergård, A. & Stolt, M. Industrual production of high molecular weight poly(lactic acid). In: Auras, R. A., Lim, L-T., Selke, S.E.M., Tsuji, H. (ed.). Poly(lactic acid): Synthesis, Structures, Properties, Processing, and Applications. New Jersey 2010, John Wiley & Sons, Inc. pp. 27–41.

[43] Avérous, L. Polylactic Acid: Synthesis, Properties and Applications. In: Monomers, Polymers and Composites from Renewable Resources. Amsterdam 2008, Elsevier. pp. 433–450.

[44] Urayama, H., Moon, S.-I. & Kimura, Y. Microstructure and Thermal Properties of Polylactides with Different L- and D-Unit Sequences: Importance of the Helical Nature of the L-Sequenced Segments. Macromolecular Materials and Engineering. 288(2003)2, pp. 137–143.

[45] Fischer, E. W., Sterzel, H. J. & Wegner, G. Investigation of the structure of solution grown crystals of lactide copolymers by means of chemical reactions. Colloid & Polymer Science. 251(1973)11, pp. 980–990.

[46] Kolstad, J. J. Crystallization kinetics of poly(L-lactide-co-meso-lactide). Journal of Applied Polymer Science. 62(1996)7, pp. 1079–1091.

[47] Wunderlich, B. Macromolecular physics. New York, USA 1980, Academic Press. 363 p.

[48] Kong, Y. & Hay, J.N. Multiple melting behaviour of poly(ethylene terephthalate). Polymer. 44(2003)3, pp. 623–633.

[49] Kim, H.G. & Robertson, R.E. Multiple melting endotherms in isothermally melt-crystallized poly(butylene terephthalate). Journal of Polymer Science Part B: Polymer Physics. 36(1998)10, pp. 1757–1767.

[50] Srimoaon, P., Dangseeyun, N. & Supaphol, P. Multiple melting behavior in isothermally crystallized poly(trimethylene terephthalate). European Polymer Journal. 40(2004)3, pp. 599–608.

[51] Ling, X. & Spruiell, J.E. Analysis of the complex thermal behavior of poly(L-lactic acid) film. I. Samples crystallized from the glassy state. Journal of Polymer Science Part B: Polymer Physics. 44(2006)22, pp. 3200–3214.

[52] Di Lorenzo, M.L. Calorimetric analysis of the multiple melting behavior of poly(L-lactic acid). Journal of Applied Polymer Science. 100(2006)4, pp. 3145–3151.

[53] Cebe, P. & Hong, S.-D. Crystallization behaviour of poly(ether-ether-ketone). Polymer. 27(1986)8, pp. 1183–1192.

[54] Bassett, D.C., Olley, R.H. & Al Raheil, I.A.M. On crystallization phenomena in PEEK. Polymer. 29(1988)10, pp. 1745–1754.

[55] Supaphol, P. Crystallization and melting behavior in syndiotactic polypropylene: Origin of multiple melting phenomenon. Journal of Applied Polymer Science. 82(2001)5, pp. 1083–1097.

[56] Yasuniwa, M., Tsubakihara, S., Sugimoto, Y. & Nakafuku, C. Thermal analysis of the double-melting behavior of poly(L-lactic acid). Journal of Polymer Science Part B: Polymer Physics. 42(2004)1, pp. 25–32.

[57] Duncan, C. & Mike, R. Principles of Differential Scanning Calorimetry. In: Thermal Analysis of Pharmaceuticals. Boca Raton 2006, CRC Press. pp. 1–21.

[58] Brown, M. E. Introduction to Thermal Analysis: Techniques and Applications. Dordrecht 2001, Kluwer Academic Publishers. 280 p.

[59] DSC 1 Product Brochure. Mettler Toledo. 14 p.

[60] Trevor, L. Optimizing DSC Experiments. In: Craig, D.Q .M . & Reading, M. (ed.). Thermal Analysis of Pharmaceuticals. Boca Raton 2006, CRC Press. pp. 23–51.

[61] Riesen, R., Widmann, G. & Truttmann, R. Alternating thermal analysis techniques. Thermochimica Acta. 272(1996)0, pp. 27–39.

[62] Simon, S.L. Temperature-modulated differential scanning calorimetry: theory and application. Thermochimica Acta. 374(2001)1, pp. 55–71.

[63] Schubnell, M., Heitz, C., Hütter, T., Sauerbrunn, S. & Schawe, J.E.K. . A Multifrequency TemperatureModulated Technique For DSC. American Laboratory. 38(2006)1, pp. 18–21.

[64] Verdonck, E., Schaap, K. & Thomas, L.C.A discussion of the principles and applications of Modulated Temperature DSC (MTDSC). International Journal of Pharmaceutics. 192(1999)1, pp. 3–20.

[65] Vicky, K., John, M., Duncan, C. & Mike, R. Modulated Temperature Differential Scanning Calorimetry. In: Craig, D.Q .M . & Reading, M. (ed.). Thermal Analysis of Pharmaceuticals. Boca Raton 2006, CRC Press. pp. 101–138.

[66] Fraga, I., Montserrat, S. & Hutchinson, J. TOPEM, a new temperature modulated DSC technique. Journal of Thermal Analysis and Calorimetry. 87(2007)1, pp. 119–124.

[67] Schawe, J. E. K. TOPEM® - The new multi-frequency temperature-modulated technique. Thermische Analyse Usercom. 22(2005)pp. 6–8.

[68] Fraga, I., Hutchinson, J. & Montserrat, S. Vitrification and devitrification during the non-isothermal cure of a thermoset. Journal of Thermal Analysis and Calorimetry. 99(2010)3, pp. 925–929.

[69] Haugen, F. Discrete-time signals and systems. Skien 2005, TechTeach. p. 75.

[70] Schawe, J. The separation of sensible and latent heat flow using TOPEM®. Mettler Toledo UserCom. 22(2005)2, pp. 16–19.

[71] Schawe, J.E.K., Hütter, T., Heitz, C., Alig, I. & Lellinger, D. Stochastic temperature modulation: A new technique in temperature-modulated DSC. Thermochimica Acta. 446(2006)1–2, pp. 147–155.

[72] Senden, D. J. A. Capturing the mechanical aging kinetics by thermal analysis. 2006. The Netherlands, Eindhoven University of Technology. Internal report. 26 p.

[73] Parmentier, L. TOPEM, a new temperature modulated DSC technique: A critical review. Master thesis. Düsseldorf 2009. University of Düsseldorf, Institute for pharmacheutical technology and biopharmacy. 45 p.

[74] Andrea, H., Renate, H., Mathias, S., Günter, S. & Andreas, F. Fourier Transform Infrared Spectroscopy. In: Li, H. (ed.). PEM Fuel Cell Diagnostic Tools. Boca Raton 2011, CRC Press. pp. 369-379.

[75] Silverstein, R. M. W., F. X. Spectrometric Identifation of Organic Compounds. New Jersey 1998, John Wiley & Sons, Inc. 496 p.

[76] Braun, B., Dorgan, J. R. & Dec, S. F. Infrared Spectroscopic Determination of Lactide Concentration in Polylactide: An Improved Methodology. Macromolecules. 39(2006)26, pp. 9302–9310.

[77] Kampert, W. G. & Sauer, B. B. Temperature modulated DSC studies of melting and recrystallization in poly (oxy-1,4-phenyleneoxy-1,4-phenylenecarbonyl-1,4-phenylene) (PEEK). Polymer Engineering & Science. 41(2001)10, pp. 1714–1730.

[78] Wunderlich, B. One hundred years research on supercooling and superheating. Thermochimica Acta. 461(2007)1–2, pp. 4–13.

[79] Toda, A., Hikosaka, M. & Yamada, K. Superheating of the melting kinetics in polymer crystals: a possible nucleation mechanism. Polymer. 43(2002)5, pp. 1667–1679.

[80] Okazaki, I. & Wunderlich, B. Reversible Melting in Polymer Crystals Detected by Temperature-Modulated Differential Scanning Calorimetry. Macromolecules. 30(1997)6, pp. 1758–1764.

[81] Okazaki, I. & Wunderlich, B. Reversible local melting in polymer crystals. Macromolecular Rapid Communications. 18(1997)4, pp. 313–318.

[82] Gonçalves, C. M. B., Coutinho, J. o. A. P. & Marrucho, I. M. Optical Properties. In: Poly(Lactic Acid). 2010, John Wiley & Sons, Inc. pp. 97–112.

[83] Kister, G., Cassanas, G. & Vert, M. Effects of morphology, conformation and configuration on the IR and Raman spectra of various poly(lactic acid)s. Polymer. 39(1998)2, pp. 267–273.

[84] Baltazar-y-Jimenez, A. & Sain, M. Effect of bismaleimide reactive extrusion on the crystallinity and mechanical performance of poly(lactic acid) green composites. Journal of Applied Polymer Science. 124(2012)4, pp. 3013–3023.

[85] Davis, E. M., Theryo, G., Hillmyer, M. A., Cairncross, R. A. & Elabd, Y. A. Liquid Water Transport in Polylactide Homo and Graft Copolymers. ACS Applied Materials & Interfaces. 3(2011)10, pp. 3997–4006.